2. Chapter 2: The Glass Transition: Comparison of the Supercooled Liquid and the Kinetically Arrested Glass

2.1. Introduction

Interest in valence-limited materials is growing, due to both their unique behaviors and their potential to form self-assembled materials with highly controlled physical properties. Despite length scales which differ by orders of magnitude, from atomic[4, 85, 86] and molecular [5, 72, 87] fluids to polymeric[88] and colloidal systems[7], these materials share common structural and dynamic features. They are all characterized by intermolecular potentials in which anisotropic interactions prevent high density conglomerates, instead allowing for more open and organized network formation[7]. These potentials describe unique and important molecular materials such as water, silica[89] and silicon[4]. The 'lock and key' specificity of natural motifs allows DNA[3, 90] and proteins[3, 91] to form anisotropic, networked structures. Directional anisotropic interactions can also be an emergent characteristic in systems after a conformational change. Examples include polymer-grafted nanoparticles[92] and low-molecular mass gelformers[93], proteins and DNA which assemble into fibers[8]. Additionally, the phase diagrams of a subset of these systems, those that form gels[3, 13, 29, 90, 94, 95, (Appendix D)], seem to be influenced primarily by the specific number of possible nearest neighbors[6], suggesting that design of novel materials can be predicted from general principles. Our strikingly simple T-shaped molecular model captures the behavior of this diverse class of materials well[1].

The phase diagram presented in our previous work demonstrated that valence-limited systems can form a wide range of materials influenced not only by the equilibrium characteristics, but also by kinetic arrest. The T-shaped molecular model includes simple liquids, gels, glasses, foams and colloidal solutions in different regions of the phase diagram dependent in part on the quenching conditions. We use the term 'molecule' to describe our elementary bonding unit; however, our model could equivalently represent an abstraction of an atomic, molecular, polymeric or colloidal system. As we seek to understand this class of materials, we must grapple with the thermodynamic and kinetic features of dynamic arrest in the high density region. Particularly, we need to consider the nature of the glass transition as it pertains to this system.

All materials, under the appropriate experimental conditions, can be supercooled below their normal melting temperature and arrested in an amorphous state on the observed timescale. Many material properties change as the glass transition temperature, T_g, is approached due to a dramatic slowing in the molecular motion and an increase in the relaxation time, τ. One of the most interesting features of supercooled liquids is that the relaxation processes become non-exponential. Near T_g the response function, $\phi(t)$, is well fit by the Kohlrausch-Williams-Watts (KWW) equation:

$$\phi(t) = e^{-\left(t/\tau\right)^{\beta}} \tag{1}$$

The value of the stretching exponent β generally decreases from 1, or simple exponential behavior, as the temperature is lowered. This behavior is also observed in gel forming materials[96].

The temperature dependence of τ near T_g has often been used to classify glass formers[64]. 'Strong' materials show nearly linear behavior on an Arrhenius plot of $\log(\tau)$ as a function of inverse temperature. Conversely, 'fragile' materials exhibit non-linear, super-Arrhenius, activation energy growth as the temperature decreases[67]. Usually, fragile liquids have a smaller value of β than strong liquids[97].

At high temperatures, simple liquids are Arrhenius in nature. As they are quenched, they reach a temperature, T_{onset}, below which there is the onset of a more fragile regime. In a number of systems there is an apparent return to Arrhenius behavior at very low temperatures referred to as the fragile-to-strong crossover (FSC)[3, 5, 72, 89, 98-102]. In addition to these dynamic properties, it has been shown that there is an inflection point in the configurational entropy, $s_c(T)$, near T_{FSC}. If we were to extrapolate the $s_c(T)$ from temperatures above the FSC, then we would find a finite temperature or 'Kauzmann' temperature, T_K, at which $s_c(T_K)=0$. Below T_K, the entropy of the liquid would be less than that of a crystal resulting in a violation of the third law as $T \to 0$[19], commonly known as the 'Kauzmann Paradox'[38]. However, the inflection point may avoid this result, instead leading to $s_c(T)>0$ for all temperatures[89]. Valence-limited systems have also been also shown to have C_v maxima, or inflections in $s_c(T)$, at all densities in the phase diagram. Whether this universally reflects a structural change is not clear[7]; however, there is compelling evidence that structural changes in colloidal systems with patchy interactions are related to the maximum in heat capacity[40, 91].

We have previously identified two factors that contribute to the rich phase behavior of the T-shaped model: local arrangements that lead to stable structures on microscopic length scales and degenerate energy minima on the potential energy landscape (PEL). Degenerate

ground states are a general characteristic of limited valency systems[7]. Under the PEL paradigm[103, 104], a system is described as a point moving along a hyper-dimensional surface. If the simulation sample is at equilibrium, the probability that the system will occupy a specific location on the PEL is determined only by the thermodynamics. In both equilibrium and arrested systems, the transition states between minima on the surface defines the motion kinetics and as well as the dynamic response.

A variety of explanations have been posed for the origin of the FSC transition. As in the case of the glass transition, we can broadly group these descriptions into those with a kinetic basis and those which suggest an underlying thermodynamic cause. From either perspective, a rough overview is coming to light. Couched in the perspective of the PEL, near T_g the energy required to overcome the energetic barriers between minima becomes significant. Additionally, the system may be unable to explore the full landscape due to the lack of mobility of near-neighbors, reducing the configurational entropy. The confluence of these effects leads to super-Arrhenius temperature dependence in this regime. At the lowest temperatures, the system becomes energetically trapped or structurally frustrated in a single basin or region of basins such that configurational entropy is nearly temperature independent. Only energetic terms contribute to the relaxation time dependence on temperature, which becomes Arrhenius again. Strong glass properties such as simple exponential behavior of the correlation function, appear to be connected to elementary local independent process of bond breaking[7]. Inherent in this description is a reduction in configurational entropy as the exploration of the surface becomes limited, and regions may become inaccessible.

Kinetically constrained descriptions of glassformers describe facilitated motion of the molecule based on the mobility of the near-neighbors. Above T_{FSC} hierarchical dynamics

dominate, requiring multiple near-neighbors to obtain certain configurations before moving. At lower temperatures only infrequent single, isolated activation steps lead to diffusive motion[28]. The higher temperature dynamics are thus the result of cooperative motion, leading to fragile characteristics, while the lower temperature dynamics are the result of individual rearrangements and, thus, return to diffusive motion and strong behavior. From this viewpoint, it is the kinetics of the model that lead to the thermodynamic and structural properties[28]. It is interesting to note that this model depends on the formation of defects which at low temperature have a concentration proportional to the energy, matching our prediction for the T-shape model[1].

Alternately, it has been noted that there are a vanishing number of defects at low temperature in network glass formers, often with a dramatic threshold or 'cutoff' of the density of states at the FSC[89]. This suggests that the PEL has a large gap between higher temperatures, where there are many locally metastable configurations, and low temperatures with limited configurations that met bond requirements. This observation may be a result of a buried phase transition[105]. Of particular note is a speculated buried liquid-liquid coexistence line in systems with potentials that facilitate both a high density isotropic liquid phase and a low density networked liquid phase[5, 36, 106]. The 'Widom line', which is a continuation of the coexistence line past the critical point and into the one phase region of the phase diagram, reflects the asymptotic convergence of response functions close to the critical point due to their common reliance on the correlation length. A system crossing the Widom line upon cooling will not demonstrate the discontinuity in the measured characteristics associated with a phase transition, but will still exhibit a dramatic change. The result is that the response function maximum, in our case C_v, marks thermodynamically the FSC[5, 72]. It

has been suggested that different classes of glass formers may be characterized by the shape and magnitude of C_v as well as its relative location with respect to the melting temperature of the liquid[107].

An example of a buried liquid/liquid phase transition can be found, in valence controlled atomic glass formers (e.g. in MD simulations of a modified Stillinger-Weber potential[85] for tetrahedral silicon[4], as well as in a germanium experimental system[86]) where there is a liquid/liquid transition such that the coexistence shifts from a single liquid metastable with respect to the crystal phase to two liquids, one of which is structurally similar to the crystal. This liquid immediately crystallizes resolving the Kauzmann paradox[4].

It has been postulated that there is a phase transition in trajectory space, as opposed to configurational space[108]. The premise is that the order parameter that should be evaluated is the trajectory of a system on the configuration manifold of the PEL. As the system becomes increasingly correlated in motion on the PEL, a first-order phase transition takes place between trajectories that remain ergodic and those that are non-ergodic[108, 109]. While no thermodynamic variables are specifically causal to this transition, there is a direct relationship to the features of the PEL[108]. Along a similar line of thought, tree representations of the PEL have been helpful in evaluating pathways towards low energy minima[110]. Wales and Bogdan created the discontinuity or tree graphs for several Lennard-Jones (LJ) potentials to demonstrate the entropic funneling could direct the state of the system, as is reflected in the heat capacity calculations[110].

Spatial heterogeneity with regard to dynamic phenomena has been well documented in both simulations and experiments of glassy systems[87]. The correlation functions of glass-like materials are often well described by a stretched exponential fit, pointing to the likelihood of

a superposition of relaxation phenomena. This leads to the assumption of different local environments which would accommodate this range in values. Empirically, the Vogel-Tammann-Fulcher (VTF) is often used to describe the temperature dependence of the dynamics for fragile glasses:

$$\tau = \tau_o e^{\left(\frac{D}{T-T_o}\right)} \tag{2}$$

It is mathematically equivalent to the Williams-Landel-Ferry equation used in polymer science[64, 111]. The accuracy of this fit in so many systems suggests that the presence of a characteristic temperature T_o, at which the relaxation time would diverge, has a physical origin. This result inspired an early theory by Adam and Gibbs[69], which defines the glass transition as a loss of ergodicity due to growing cooperatively rearranging regions, described by the size of energy fluctuations required to allow a group of particles to collectively relax into their local equilibrium. Other more recent theories and models build on this work, utilizing some form of spatial partitioning of the system[27, 68]. There is growing experimental and theoretical evidence that material dynamics are very different in regions only a few nanometers apart at temperatures near the glass transition. An excellent review of spatial heterogeneity by Ediger[97] captures a variety of results from experimental and simulated systems, as well as potential explanations. Of note, it is not clear whether the spatial heterogeneity is a result or cause of the dynamic heterogeneity. There is no apparent structural cause for these cooperative regions as a liquid is supercooled. X-ray and neutron scattering studies only show small changes in local packing even in samples with viscosity changes of 12 orders of magnitude[97]. Our model gives us insight into the spatial dynamics of a prototypical example of valence-limited glasses, hopefully lending further information towards this fundamental question.

Within this chapter we extend our work with the T-shaped molecule model to include not only structural, but also dynamic information collected from simulation samples. A paucity of low temperature measurements hinders attempts to understand the fragile-to-strong Crossover (FSC)[102, 112]. Exploration of valence-limited systems have also been inhibited by the inability to access low temperatures[113]. Our work, which captures low temperature supercooled equilibrium states as well as kinetically arrested states, sheds some light on these questions. After defining the model in the appropriate context in Section 2, we describe the simulation methods used in Section 3. We then analyze the equilibrium liquids structure and dynamics in Section 4, and compare these with the kinetically arrested, non-equilibrium, glass formers reported in Section 5. In Section 6, evidence of structural heterogeneity in the equilibrium system is presented. We end this chapter with a discussion of our results to date and a brief summary of our conclusions.

2.2. Definition of T-shaped Molecule Model

The T-shaped molecule occupies the vertex, located at $\vec{i}$ on a square lattice, a model we previously described[1]. Each T-shaped molecule, σ_α, has three bonding sites which lie in a plane, resulting in 4 possible orientations, $\alpha = 1, 2, 3$ or 4. When the T-shaped molecules at two neighboring vertices, $\langle \vec{i}, \vec{i}\,' \rangle$, are oriented such that they each have bonding sites along the same edge, we define the resulting connection to be a bond which leads to a favorable energetic interaction. Else, there is no interaction.

Our simulation samples are in the fully-dense region of the phase diagram where every vertex is occupied by a molecule. While the density of T-shaped molecules (1 per vertex) is

a conserved quantity, the density of bonds is not. Instead, the density of bonds is strongly influenced by the temperature. In the limiting case of high temperature, the bond density is 9/8 per vertex on a square lattice[114]. As the temperature goes to zero, the bond density approaches 3/2 per vertex.

For convenience and clarity, we restate the Hamiltonian for the fully-dense lattice:

$$\beta H(t) = {}^{-\beta\varepsilon}\!/_{2} \sum_{\langle \vec{i},\vec{i}\,' \rangle} \sigma_{\alpha}\left(t;\vec{i}\right)\sigma_{\gamma}\left(t;\vec{i}\,'\right) \tag{3}$$

where

$$\sigma_{\alpha}\left(t;\vec{i}\right)\sigma_{\gamma}\left(t;\vec{i}\,'\right) = \begin{cases} 1 \text{ if both molecules have bonding} \\ \quad \text{sites along the shared edge } \left\langle \vec{i},\vec{i}\,' \right\rangle \\ 0 \text{ otherwise} \end{cases} \tag{4}$$

the Greek subscripts indicate the orientation of the molecule($\alpha = 1,2,3$ or 4), t indicates that the orientation may be different at different times, and the sum is over all shared edges (near-neighbors pairs). The temperature is expressed in reduced units $T^{*} = \left(\beta\varepsilon\right)^{-1}$. We omit the asterisks in the following text for convenience. All simulation samples studied are 128 vertices by 128 vertices with periodic boundary conditions. This is much larger than any spatial correlation found within the simulation samples themselves.

In previous work (Section 1.4.3)[1], we reported the transition temperature under the mean-field approximation as $T_{mf,critical} = (3\log 3)^{-1}$ with the supercooled stability limit of $T_{mf,spinodal} = 1/4$. In the following sections and discussion, we will identify other temperatures of interest. However, these transition temperatures provide a reference point during our work.

2.3. Simulation Methods

The glass transition is, by its very nature, controlled by the interplay of the thermodynamics and kinetics of the material. One powerful description of this interrelation is the energy landscape paradigm. We can visualize all possible states of the lattice as defining a hyper-dimensional PEL (albeit discrete) in conformational space. A specific state of the system (our simulation sample) m is located on the PEL at the conformation coordinate $\vec{x}_m$, where $\vec{x}_m \equiv \left\{\sigma_{\alpha_1}\left(\vec{i}_1\right), \sigma_{\alpha_2}\left(\vec{i}_2\right), \cdots, \sigma_{\alpha_N}\left(\vec{i}_N\right)\right\}$. The numerical subscripts specify individual molecules, σ, in orientation α and location $\vec{i}$ on the square lattice. The energy at $\vec{x}_m$, E_m,is defined by the Hamiltonian and motion along the surface to a new coordinate $\vec{x}_k$ occurs by the change in orientation of a single molecule.

The energy at each state, however, only defines the intrinsic thermodynamics of the system. We must also incorporate the appropriate transition probabilities $q_{k\to m}$ between states such that at long-time ($t \to \infty$) the probability that a simulation sample is found in state m, p_m, reflects the canonical distribution. (All our simulations were performed using the canonical ensemble with our simulation samples coupled to a thermal bath.) In Section 2.3.1, we will find that there are many choices of $q_{k\to m}$ which could satisfy the requirement and lead to the appropriate distribution. We employ two different Monte Carlo (MC) simulation techniques with their associated transition probabilities in our work.

The first is a modified Metropolis MC recipe, as described in Section 2.3.2, with which we indentify the low temperature 'equilibrium' conditions. If we wish to explore the kinetic properties of our model and collect dynamic information, we must also define the physically appropriate transition states $\vec{x}^*_{m\to k}$ for our model. The choice of $q_{k\to m}$ is now further

restricted to incorporate the energetic impact of these transition pathways. Residence time kinetic Monte Carlo (kMC) incorporating both the use of the landscape description to find the transition probabilities and a technique to improve the speed of the simulation is described in Section 2.3.3. Further description of these methods can be found in Appendix E.

2.3.1. Master Equation

As the equilibrium probabilities are not known *a priori*, we use the master equation formalism such that any initial distribution explores conformation space according to the dynamic path[115]:

$$\frac{dp_m(t)}{dt} = \sum_k q_{k\to m} p_k(t) - \sum_k q_{m\to k} p_m(t) \tag{5}$$

The transition probabilities, $q_{k\to m}$, specify the rules of motion along the landscape from $\vec{x}_k$ to $\vec{x}_m$. At long-times, steady state should be reached, so the left hand side of (5) must go to zero and the probabilities $p_k(t)$ and $p_m(t)$ adopt their equilibrium value. This results in the condition of detail balance with:

$$q_{k\to m}\exp\left(-\beta E_k\right) = q_{m\to k}\exp\left(-\beta E_m\right) \tag{6}$$

We notice that the choice of transition probabilities is not unique. As is often the case, even our simple model does not result in an analytically tractable master equation. Instead, we find the dynamic and equilibrium properties by creating a lattice 'sample' and using Monte Carlo (MC) simulations to evolve this sample in time[46, 116].

2.3.2. Metropolis Monte Carlo Simulations

As mentioned above, two different MC simulation methods were employed for these studies. First, a modified Metropolis recipe[117] was employed for equilibration of the lattices. Under the modified Metropolis algorithm, the probability of acceptance is a comparison of the initial and final states only. Although the rate of change of breaking a single bond increases exponentially with decreasing temperature, all transitions to lower or degenerate energy states are accepted (see Figure E-1). The acceptance rate for this method was sufficiently large to cool to very low temperatures relative to the predicted mean-field transition. Thus, the method allows for a simulation sample to explore a large number of configurations quickly from a computational stance.

In our implementation, we challenge an individual molecule with a random transition from its current orientation to a new orientation chosen at random. The acceptance of the new orientation or return to its original orientation completes the move. We define one Monte Carlo step (MCS) to be equal to the same number of challenges as there are vertices on the lattice. However we select the molecule for the move randomly, so in one MCS not every vertex on the lattice may be challenged. While the time step for each Monte Carlo attempt under this recipe does not have an explicit connection to real time, and therefore the dynamics do not have a clear definition, we note at equilibrium the distribution of states is expected to be canonical and the conditions of detail balance is met[118, 119]. We consider the Metropolis results to represent the true equilibrium description of the system, an assumption supported by results (see Section 2.4.1).

2.3.3. Kinetic Monte Carlo Simulations

In addition to the two conditions described by (5) and (6), extracting dynamic details via residence time kinetic Monte Carlo (kMC) simulation- also known as the 'n-fold method'- requires us to define the conformational surface between $\vec{x}_m$ and $\vec{x}_k$ for all states m and k [118]. The transition state energy, $E^*_{m\to k}$ at $\vec{x}^*_{m\to k}$ describes the energy barrier to the change in state. The transition probabilities $q_{m\to n}$ reflect the potential energy difference between $\vec{x}_m$ and $\vec{x}^*_{m\to k}$

$$q_{m\to k} = \omega \exp(-\beta(E^*_{m\to k} - E_m)) \tag{7}$$

where ω^{-1} becomes the fundamental time scale which encompasses all faster relaxation process due to thermal vibrations within the energy well that our coarse grain model neglects. Conveniently, because each state is linked via the rotation of a single molecule $\sigma_\alpha\left(\vec{i}\right)$, we define $E^*_{m\to k} - E_m$ as the number of bonds that specific molecule had at state m, which must be broken to move to the new state. Notice that there is no impact of the final orientation of that molecule on the transition probability. This choice also meets the requirements of detail balance.

The traditional importance method, proposing a new state and then accepting, or rejecting, that move based on comparison with a random number, is inadequate at low temperature because of the large number of rejected moves[46]. Instead, we found the n-fold, or residence time [118, 120, 121], technique to be very effective. In this technique, every event is accepted and the time between events is weighted by the total probability of moves.

2.4. Supercooled Liquid: Investigation of Equilibrated Samples

Using the modified Metropolis recipe, we are able to quench to very low temperatures, creating simulation samples which are in an equilibrium state. We use the term equilibrium to denote samples which reflect path-independent quantities, which are characterized by the current conditions regardless of previous temperature history. In this section, we will present results that establish that the MC samples are at equilibrium, and then use these equilibrated samples as the initial point for both thermodynamic and kinetic calculations.

We note that while we can calculate a first-order, mean-field liquid to solid transition temperature $T_{mf,binodal}$, the significance of the melting temperature and the order of the actual transition are not clear from the outset. One objective is to ascertain the differences between the equilibrium behavior and the non-equilibrium behavior. For the purposes of this work and consistency with other sources, we will refer to all simulation samples as supercooled liquids without regard to the implication of metastability with respect to a solid. In a similar fashion, all simulation samples that deviate from equilibrium at long-time, as described in Section 2.5, will all be classified as glasses without specific demonstration of dynamic arrest.

2.4.1. Equilibrium Results from Metropolis MC Method

The simulation samples that are quenched initially via the Metropolis recipe do indeed appear to reflect an equilibrium state, with similar energetic and structural length scales of low temperature simulation samples that are quenched with the kMC method. The Metropolis recipe does not provide dynamic information, but does search the PEL more rapidly because there is no energetic barrier for transition beyond the difference in the number of bonds in initial and final states. If we are able to access a large number of

configurations during our simulation time, then we have the ability to meet the conditions of equilibrium described by equation (6). We noted that the measured acceptance rate, the percent of MCS that represents motion on the PEL, remains sufficiently high even at low temperature implying that we are, indeed, capable of meeting this requirement.

While we cannot formally prove that these simulations are truly the equilibrium state, evidence points to reproducible results that, excluding the initial decay, do not change in energy over long simulation periods. For all results in this section, each simulation sample was created at a unique, random, initial condition equivalent to $T \to \infty$. They were then 'quenched' by using the final temperature during all simulation moves. The samples were relaxed for at least 10^6 MCS before any data was reported. In previous work[1] we found that the Metropolis MC simulation samples had a relaxation time of less than 10^2 MCS for samples as low as T=0.18 (refer to Figure 1.6.3-1). This gives us confidence we had reached the low energy equilibrium state for each temperature. Ten separate measurements of the internal energy density, u, were recorded at intervals of 1000 MCS, from which the average was then calculated. This was repeated for a second independent simulation run with the same quench conditions but a different initial configuration. Both sets of data are reported in Figure 2.4.2-1. Two additional series following the same protocol were generated but omitted in our figure as they were not used for the fitting of u. None of the energy values differed by more than 1%.

Additionally, the simulation samples' path independence- that is, whether the states could be completely defined by the current conditions regardless of previous thermal history- was also investigated. In the stepwise method, a sample was equilibrated at high temperature, then 'quenched' to the next cooler temperature, where it was equilibrated and the process

repeated (temperature steps followed those reported in Figure 2.4.4-1, so individual data points could be compared). This procedure provided a set of simulation samples that is not distinguishable from those generated during the direct quench.

As seen in Figure 2.4.2-1, the samples also approach the high-and-low temperature energy limits, as we would expect. In Section 2.4.3, we indicate the presence of the crystalline state (long range enrichment in either orientation 1 and 3 or 2 and 4) as primarily a kinetic phenomena. We note that in the absence of a crystal with lower free energy, any of the degenerate minima would be the equivalent thermodynamic equilibrium state[122]. Thus, our calculation of the configurational entropy in Section 2.4.2, which indicates that the entropy remains positive as the temperature goes to zero, is consistent with the absence of a unique state with the lowest energy. The structural ordering documented in Section 2.4.3, which occurs due to the anisotropic nature of the molecules, is not representative of a unique equilibrium state.

2.4.2. Configurational Entropy

There are several different methods to calculate the heat capacity, and thus entropy, for a simulation sample. As the model is defined on a lattice and each molecule has a discrete number of orientations, the only entropy present in our system is the configurational entropy. If our system is at equilibrium, we can use the thermodynamic relationships

$$C_V \equiv \left.\frac{\partial U}{\partial T}\right|_V , \quad s(T) = s\big|_{T=\infty} - \int_T^\infty \frac{C_V}{T} dT \tag{8}$$

where C_v is the heat capacity per site and s is the entropy per site. The entropy density at infinite temperature can be easily found using the Boltzmann definition, $s\big|_{T=\infty} = \log(4)$ as there are 4 orientations at each site.

Alternately, we could measure the heat capacity directly from our simulation results because we can measure the fluctuations in the energy, via the variance of the internal energy, as

$$C_V \equiv \frac{\left\langle \left(U - \langle U \rangle\right)^2 \right\rangle}{kT^2} \tag{9}$$

However, because of the statistical inefficiency of using the variance of the internal energy (see Appendix F), we chose to fit the data to an arbitrary function that can be differentiated analytically using Eq. (8). Hyperbolic functions were chosen because the energy has both a high and low temperature asymptote (polynomial and simple exponential expansions cannot take advantage of the two known values). We found that

$$\begin{aligned} u &= -9/8 - 3/8\left((a)\tanh\left(b/T\right) + (1-a)\tanh^2\left(c/T\right)\right) \\ &= -9/8 - 3/8\left((0.468)\tanh\left(0.375/T\right) + (1-0.468)\tanh^2\left(0.256/T\right)\right) \end{aligned} \tag{10}$$

describes our data well, with a small number of variables (note the -9/8 and -3/8 are set by the asymptotes).

In Figure 2.4.2-1 (a), we plot the data with its fit (equation (10)). As mentioned above, we use the analytic derivative of equation (10) to calculate the specific heat, shown in *(a)inset*. To insure that this choice does not deviate in a systematic way, the variance of the energy measured directly from the simulation samples employing equation (9) is shown with black dots (●). Additional confirmation is given by the close alignment of the slope of the line segment connecting adjacent energy measurements marked by the red stars (*). The entropy per site calculated from the integration of C_V / T and knowledge of the high temperature limit is shown in Figure 2.4.2-1 (b).

The equilibrium conditions generated by this Hamiltonian require that there be a peak in the heat capacity at some temperature, T_{Cv}. We draw this conclusion by considering the functional shape of the internal energy per site, u. In the high temperature limit, the thermal energy will overwhelm any resistance from bonds and explore the entire energy landscape. Thus, the internal energy will be equivalent to the energy of the random state ($u = -9/8$). As this condition is asymptotic as $T \to \infty$ and the energy decreases upon cooling, the function is by nature concave down above T_{Cv}. As a sample cools (under conditions slow enough to maintain equilibrium) towards absolute zero, the molecules will preferentially align towards a bonded condition. Therefore $u \to -3/2$ as $T \to 0$ and below T_{Cv} the internal energy function is concave up. We find this description to be consistent with all simulated conditions in this study. The maximum heat capacity occurs at $T_{Cv} = 0.21$ (recall $T_{mf,spinodal} = 0.25$).

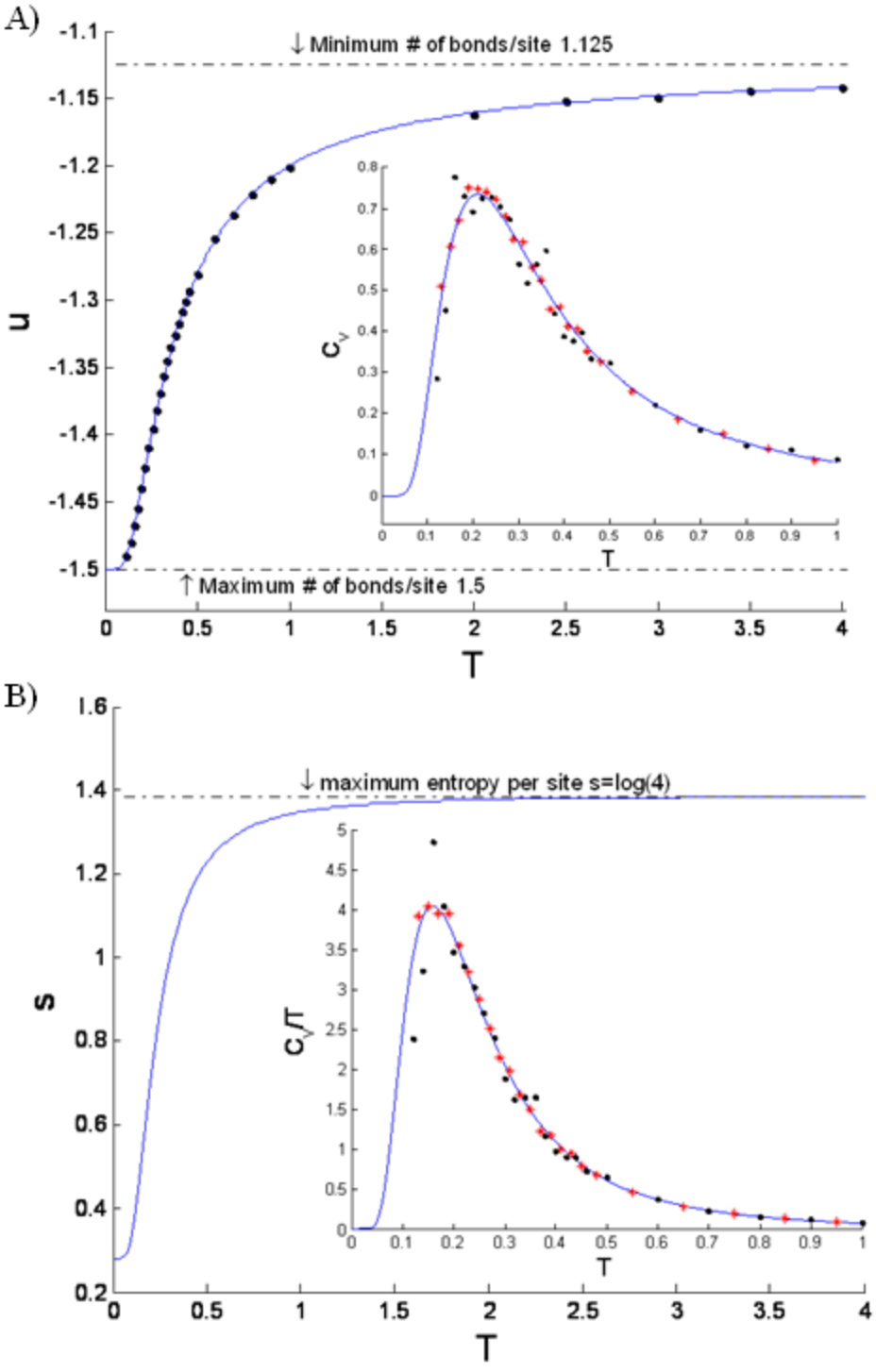

Figure 2.4.2-1: Thermodynamic features of the 'supercooled' liquid

(A) u as a function of T. The data (●) was fit to an arbitrary analytic function(—). The inset shows C_V calculated by three methods: (●) variance of the energy, (*) slope of the line segment connecting adjacent energy measurements, (—) the analytic derivative. (B) s (—) calculated from the integration of C_V/T and knowledge of the high temperature limit.

We note that the greatest error in calculating entropy occurs in the low temperature measurements, when relaxation times are the longest, as one would expect. Computational limitations have precluded other investigations from achieving low temperature results[123]; we are fortunate to have a simple model and technique to overcome this difficulty. However within this error our calculations still suggest a positive residual entropy, a result that has also been found in an experimental system[124]. This quantity can only be reasonably extrapolated from low temperature equilibrium conditions. There is very active research into the applicability and definition of thermodynamics and statistical dynamic quantities in the immediate vicinity of $T = 0$, which are beyond the scope of this work[125, 126].

If the configurational entropy of the glass does not go to zero as temperature goes to zero, the extrapolated inversion of the liquid and crystal entropies is not thermodynamically mandated. This provides a resolution to the 'Kauzmann Paradox' for our system without the need for a thermodynamic or dynamic event at lower temperatures. Indeed, it questions the universal applicability of the assumption that one may calculate the 'ideal glass transition' based on extrapolations of the configurational entropy to $s_c = 0$.

2.4.3. Structure

Because of the system anisotropy, there is noticeable ordering as the temperature is lowered. The anisotropic nature of the molecules leads to the formation of 'back-to-back' pairs so that the non-bonded sides of the molecules face each other. Structures in the same direction as the long axis of the molecule are formed. The result is local enrichments of molecules whose long axis is oriented in the same direction ($\alpha = 1,3$ or $\alpha = 2,4$). Measurements of simulation samples at different temperatures show a pronounced increase in the size of these domains at colder temperatures.

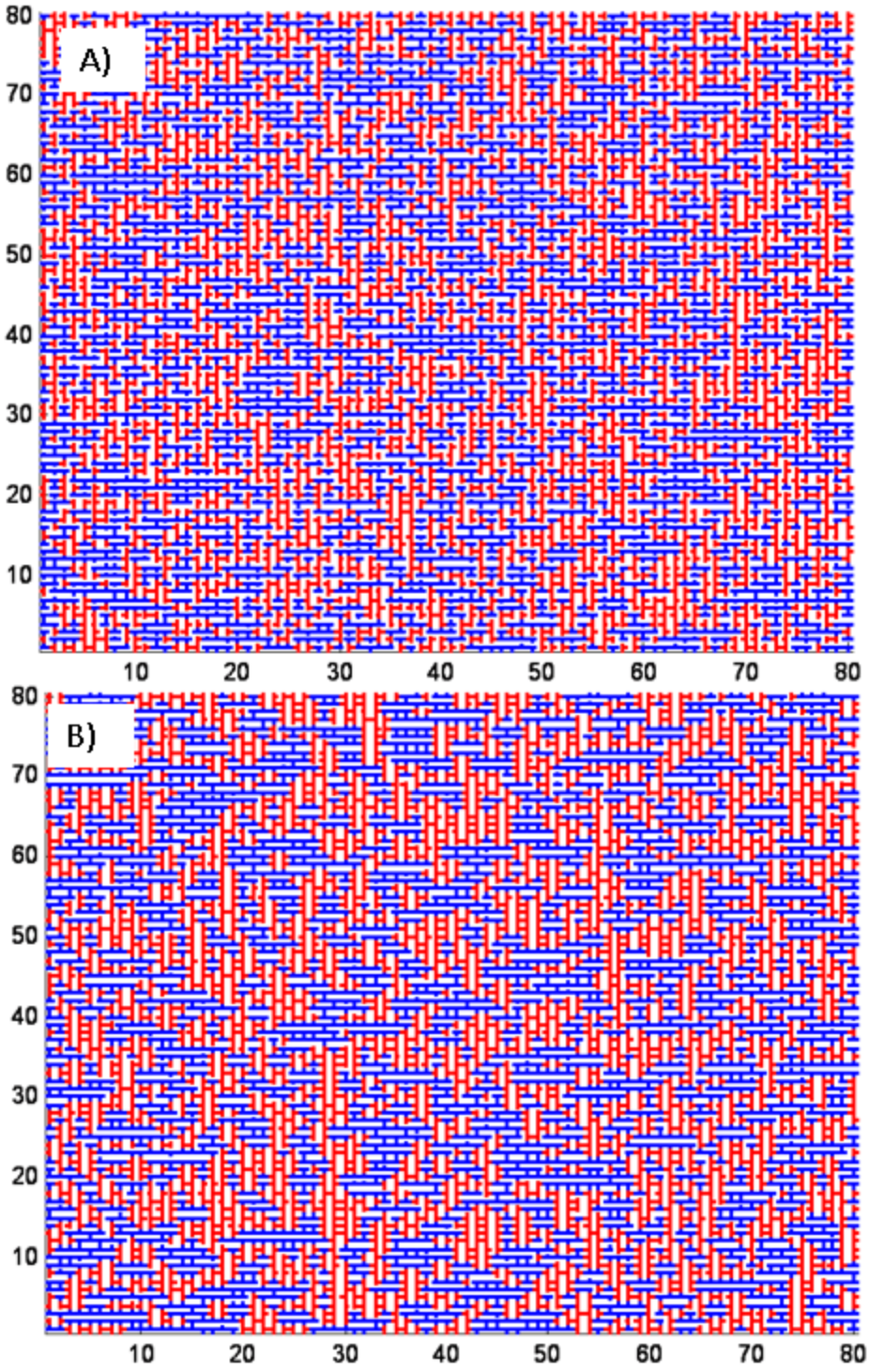

Figure 2.4.3-1: Representative snapshots of simulation samples
Supercooled liquid simulation samples at (A) T=1.0 and (B) T=0.20 . Coloring is a guide to the eye to distinguish orientations 1 ⊢ and 3 ⊣ from 2 ⊤ and 4 ⊥ .

Given that there is a kinetic preference for an aligned system (described in Section 1.4.5), which we intuitively relate to the ordered crystalline state, why do we not observe the

macroscopic crystal in the MC samples? When we used the dynamic mean-field (DMF) simulation to cool a sample which had a small fluctuation at a temperature very close to the transition temperature, we indeed did see a crystalline structure[1]. The nature of the DMF simulation as a method of steepest decent is such that once it finds one energy minimum, it does not continue to explore the configuration space. The small kinetic preference toward the alignment leads to formation of a long range structure when only a single disturbance is introduced. In contrast, either form of the MC simulation permits the sample to explore a wide range of energy minima at this temperature, most of which have minimal ordering. (Due to the anisotropic nature, there is ordering on a small-length scale congruent with the need for the 'back-to-back' alignment for bond formation.) Recently Ediger et al. [127] posited that the kinetic rate of crystallization is proportional to the rate of discovery of crystalline configurations on the PEL. In our model, the overwhelming number of non-aligned minima would make crystallization unlikely.

We are able to see clear regions with local enrichments of molecules whose long axis is oriented in the same direction ($\alpha = 1,3$ or $\alpha = 2,4$). These regions grow with decreasing temperature, despite their kinetic origin, due to the stabilization of the bonds within their boundaries. Rotation of a molecule to a different orientation would raise the energy of the simulation sample by at least one bond, possibly two.

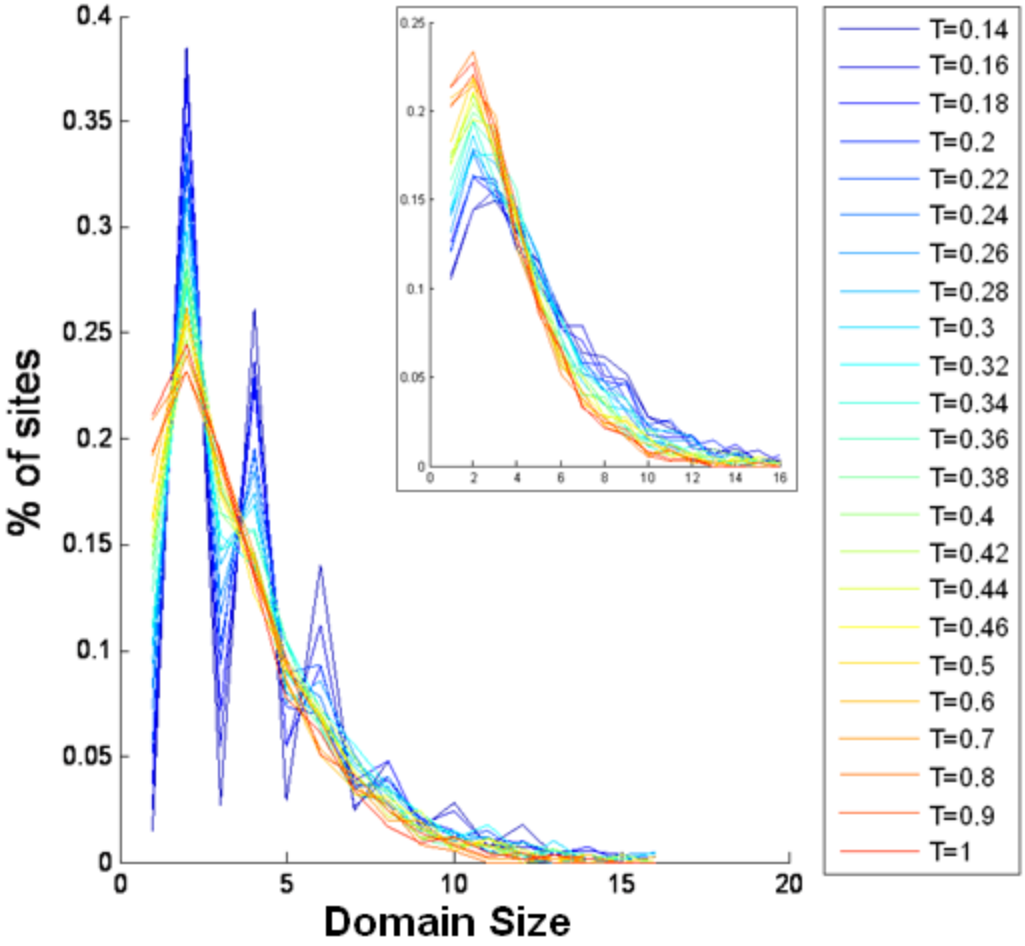

Figure 2.4.3-2: Distribution of domain size at different temperatures
The anisotropic ordering is pronounced when the length of rows/columns in the enriched regions are measured in the direction of the long axis (inset: domain length measured in perpendicular direction).

The local enrichments demonstrate the model's tendency toward reversible self-assembly. Indeed, a number of other anisotropic or limited valence models and materials share this characteristic that local homogeneous patches stabilized by a network of intermolecular bonds [e.g.7, 90 and references therein]. Due to the small length scale of these regions with respect to the lattice spacing, measurements along the axis in a linear direction are significantly more revealing than the traditional radial distributions and structure factors. We have chosen the expectation value of the domain size, or length scale of local enrichment of either the 1 ├ and

3 ┤ or 2 ┬ and 4 ⊥ orientation, as a convenient representation of the degree of orienting. In Figure 2.4.3-3 we can clearly see that there is an onset of increased orientation at approximately $T_{structure} = 0.5$, but that there does not seem to be any signature of divergence in this length scale as $T \to 0$. It is important to note that there are approximately an equal number of molecules in each orientation within a sample during the duration of the simulation. The locally oriented regions do not necessarily indicate an underlying phase transition due to a symmetry breaking in orientation.

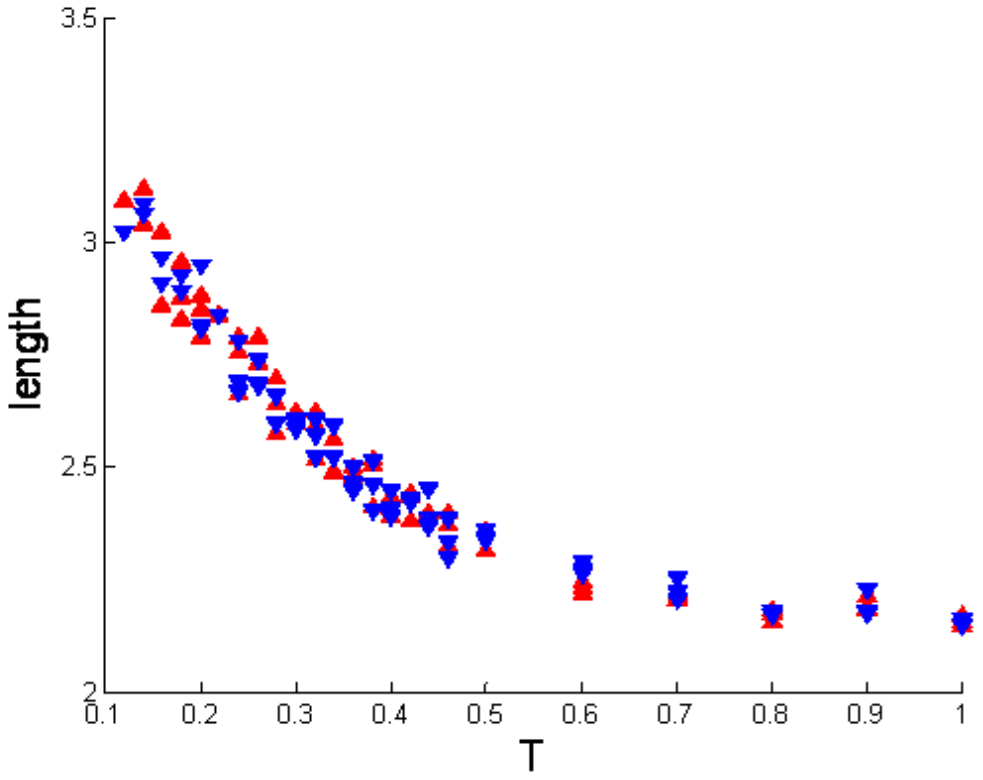

Figure 2.4.3-3: Expectation value of the domain size at different temperatures
The expectation value of the linear distribution in the direction of the long axis(▲) and perpendicular to the long axis(▼)

2.4.4. Relaxation Time

We employ the relaxation time as proxy for rheological measurements of the material's viscous character. Among many possible choices for the relaxation time, we explore the relaxation time for two autocorrelation functions within this work. The bond autocorrelation function, $\phi_b(t-t_o)$, comparing the bonding state of the lattice at time t to that at the time t_0 defined as:

$$b\left(t;\left\langle \vec{i},\vec{i}\,'\right\rangle\right)=\begin{cases}1:\ \text{bond along edge } \left\langle \vec{i},\vec{i}\,'\right\rangle \text{ at } t\\ 0:\ \text{no bond along edge } \left\langle \vec{i},\vec{i}\,'\right\rangle \text{ at } t\end{cases}$$

$$\phi_b(t-t_o)=\frac{\left[\left\langle b\left(t_o;\left\langle \vec{i},\vec{i}\,'\right\rangle\right)b\left(t;\left\langle \vec{i},\vec{i}\,'\right\rangle\right)\right\rangle-\left\langle b\left(t;\left\langle \vec{i},\vec{i}\,'\right\rangle\right)\right\rangle^2\right]}{\left[\left\langle b\left(t;\left\langle \vec{i},\vec{i}\,'\right\rangle\right)^2\right\rangle-\left\langle b\left(t;\left\langle \vec{i},\vec{i}\,'\right\rangle\right)\right\rangle^2\right]} \tag{11}$$

We also simultaneously evaluated the molecule-orientation autocorrelation function,

$$\sigma_\alpha\left(t;\vec{i}\right)=\begin{cases}1:\ \text{if molecule at vertex } \vec{i} \text{ is in orientation } \alpha \text{ at time } t\\ 0:\ \text{otherwise}\end{cases}$$

$$\phi_\sigma(t-t_o)=\sum_{\alpha=1}^{4}\frac{\left[\left\langle \sigma_\alpha\left(t_o;\vec{i}\right)\sigma_\gamma\left(t;\vec{i}\right)\right\rangle-\left\langle \sigma_\alpha\left(t;\vec{i}\right)\right\rangle^2\right]}{\left[\left\langle \sigma_\alpha\left(t;\vec{i}\right)^2\right\rangle-\left\langle \sigma_\alpha\left(t;\vec{i}\right)\right\rangle^2\right]} \tag{12}$$

The structural resistance and solid-like features in our simulation samples are provided by the bonding structure. As has been observed in other models[3], the local structure can reinforce the bonding along a specific edge, $\left\langle \vec{i},\vec{i}\,'\right\rangle$. Thus, a bond may break and reform quickly, returning to the original structure and not suggesting actual progress towards relaxation. Further, in our model several different orientations of the molecule at a specific site may result in the same local bonding characteristics. The results for the orientation and bond relaxation functions were very similar. As the bonding state defines the

thermodynamics and as we also use bonding to describe the structural correlation functions, we choose to report the bond relaxation function results here. Later, in Section 2.6 we will refer to the orientation times.

We evaluated the equilibrium relaxation time, τ, for the simulation samples that were created by quenching from an initial random state (infinite temperature) to the final temperature and equilibration for more than 10^6 MCS with the Metropolis method. Following equilibration, the data for the autocorrelation functions was collected using kMC simulations. As described earlier, it is important that we consider the transition states to capture appropriate motion on the energy landscape when we are directly evaluating any function involving time dependence.

There are many ways to characterize the relaxation time from the autocorrelation function results. For this work, the use of the integrated relaxation time, or mean relaxation time, is preferred because it incorporates both the influence of the characteristic time, τ_c, and the stretching exponent, β. We calculated the relaxation time by first fitting the autocorrelation function with the stretched exponential equation, $\phi(t) = e^{-\left(t/\tau_s\right)^{\beta}}$. The Euler gamma function then allows us to calculate the integral.

$$\begin{aligned} &\phi(t) = e^{-\left(t/\tau_s\right)^{\beta}} \\ &\tau = \int_0^{\infty} e^{-\left(t/\tau_s\right)^{\beta}} dt = \left(\tau_s/\beta\right)\Gamma\left(1/\beta\right) \end{aligned} \tag{13}$$

It also provides a clear connection to the relaxation time calculated by a single exponential relationship. In the simple exponential relaxation function, the relaxation time remains the

same when integrated over the interval, $\phi(t) = e^{-t/\tau}$ or $\tau = \int_0^\infty e^{-t/\tau} dt$ [38]. We found that in all cases the stretched exponential provided a better fit than a single exponential function.

The values of τ and β are reported in Figure 2.4.4-1. We monitored the decay of the correlation function and fit the data to each measurement separately to ensure that the simulation sample was exploring similar regions of the PEL and that we did not neglect a longer timescale. As the error of the integrated relaxation time τ was small (each measurement is reported separately and at most temperatures the symbols overlap), we have confidence that the reported values reflect the actual relaxation times. On the other hand, there was a larger variation in β (Figure 2.4.4-1 *inset*). Other authors often report β as nearly independent of temperature, noting that the change in the vicinity of T_g is minimal[3]. It has been noted that the value of β is very sensitive to the fitting method[128, 129]. We considered different ways to fit the data, particularly whether to include or exclude very short or long-time processes. Compared to the variance in values of τ or β between quenches at the same temperature, neither truncated data set had fitting parameters which were significantly different.

The value of β can be used as an indicator of the kinetic fragility as it represents the non-exponential movement of the simulations sample on the PEL. Indeed a dramatic change in β upon a return to simple exponential relaxation is given as the hallmark of the fragile-to-strong crossover (FSC) in a spin facilitated kinetic Ising model[129]. Despite the spread of our measurements, since we are considering the FSC, it is interesting to note that the simulation samples become more fragile as the temperature is lowered to $T_{\beta:fragility,\ onset} \approx 0.5$. The value

of β then stabilizes until it begins to increase at $T_{\beta:FSC} \approx 0.26 - 0.24$. Again, however, the specific temperatures are difficult to establish.

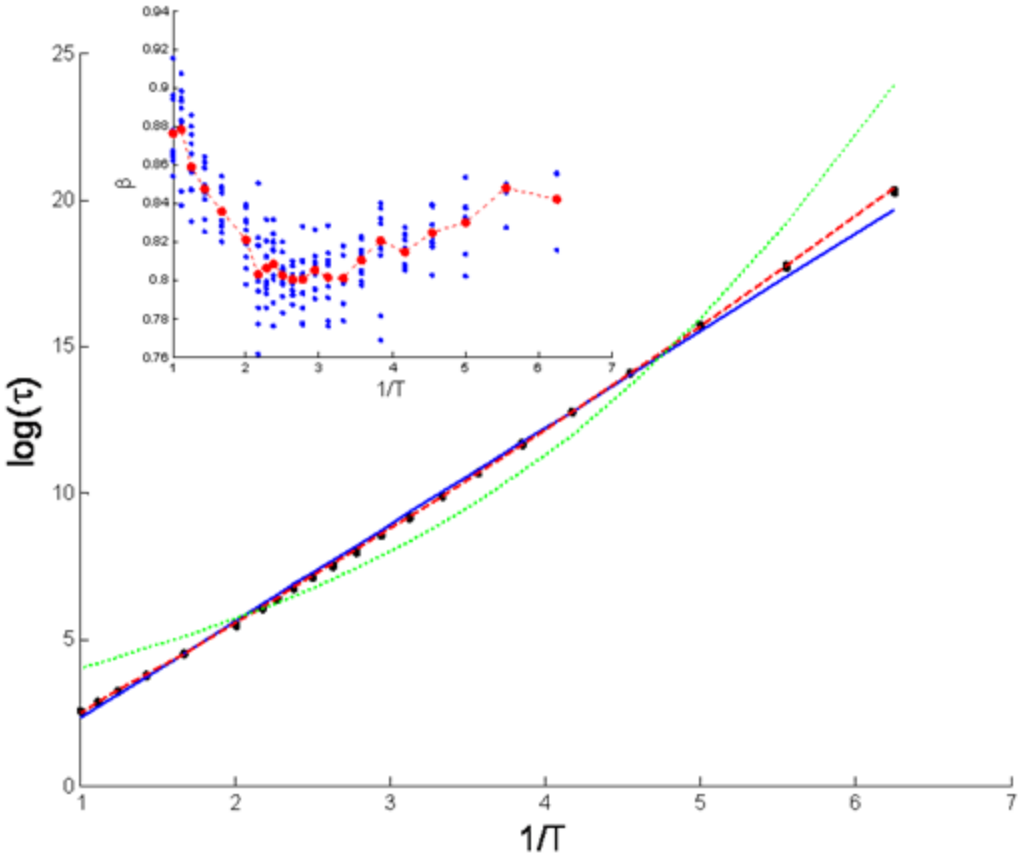

Figure 2.4.4-1: The integrated relaxation time of supercooled simulation samples
The points (•) are independent fits of relaxation runs (4 at T=0.16, 3 at T=0.18, 8 at T=0.20, 10 for all other) which overlap closely on this scale. The data is fit in to the (—) Arrhenius, (--)Vogel-Fulchur and (...) Adams-Gibbs equations. Inset: shows the (•) values of the stretched exponent β, (•) the average value and (--) as a guide to the eye. Note that while x-axis is 1/T, to match the main plot for convenience to the reader, the y-axis on the inset is linear.

The integrated relaxation time as a function of temperature was fit with four functions. As expected from the implied cooperative relaxation, the Vogol-Tammann-Fulchur function(VTF):

$$\tau = \tau_o e^{\left(\frac{D}{T-T_o}\right)} = 0.656 e^{\left(\frac{2.85}{T-0.023}\right)} \qquad (14)$$

fit the complete data set better than an Arrhenius function:

$$\tau = \tau_o e^{\left(E_a/T\right)} = 0.368 e^{\left(3.32/T\right)} \tag{15}$$

We notice that the activation energy, E_A, in the Arrhenius fit is 3.32, which is slightly larger than that which would be required to break three bonds. In regions of the system which are fully satisfied, change in orientation of a monomer requires that three bonds be broken. This represents the highest energy barrier to local relaxation. Whereas, at higher temperatures samples have a smaller bond density, the largest energy barrier may be circumvented by longer pathways over the PEL, there will be a time penalty for this diffusive motion. Therefore, while the energy scale is appropriate for both scenarios, the details of the relaxation mechanism remain unknown.

With the thermodynamic calculations made before, we are able to evaluate the fit of the Adam-Gibbs[69] (AG) equation. This equation, and the theory on which it is based, was inspired in part from the excellent empirical fit of the VTF function. If we postulated that there is a physical significance to T_o, the singularity suggests a divergent relaxation time consistent with the ideal glass transition. T_o is often then equated with Kauzmann temperature T_K.

The configurational entropy, calculated at each temperature as shown in Figure 2.4.2-1, is known, so it is not a degree of freedom in our fit for the AG equation:

$$\tau = \tau_o e^{\left(C/TS_c\right)} = 13.6 e^{\left(1.89/TS_c\right)} \tag{16}$$

The fit is relatively poor. However, if we restrict the fit to a smaller region closer to the expected glass transition, as is commonly done[128], the fit greatly improves (not shown).

Recent work suggests that the AG should also fit well if extended above the activated regime, where the s_c has little dependence on temperature[123].

Alternative relationships are also being actively proposed as the source of the relaxation behavior and the nature of T_g is investigated. Recently, Elmatad et al. proposed a quadratic fit, which could be used to collapse an impressive range of data from structural glass formers[112]. We could use this functional form to fit our data, either over the entire temperature range,

$$\tau = \tau_o e^{\left(\left(J/T_a\right)^2\left(\left(T_a/T\right)-1\right)^2\right)} = 1.48e^{\left(\left(3.32/2.28\right)^2\left(\left(2.28/T\right)-1\right)^2\right)} \qquad (17)$$

or alternately over an arbitrary subset of temperatures (no fits are shown). The physical rational behind this functional fit, based on the activation energy required to relax a domain of a particular size, limits its application to temperatures where the system movement on the energy landscape is dominated by activated, cooperative motions ($T < T_a$). Likewise, it will no longer apply when the temperature is further cooled ($T < T_x$) returning to motion without correlated transitions. The authors expected that below T_x the relaxation dynamics would return to an Arrhenius form. We did not find unique choices of T_a and T_x while attempting to fit this function to our relaxation data. However, our data is consistent with a transition into a cooperative, fragile, relaxation regime, followed by a return to Arrhenius, strong, behavior at even lower temperature, as demonstrated elsewhere.

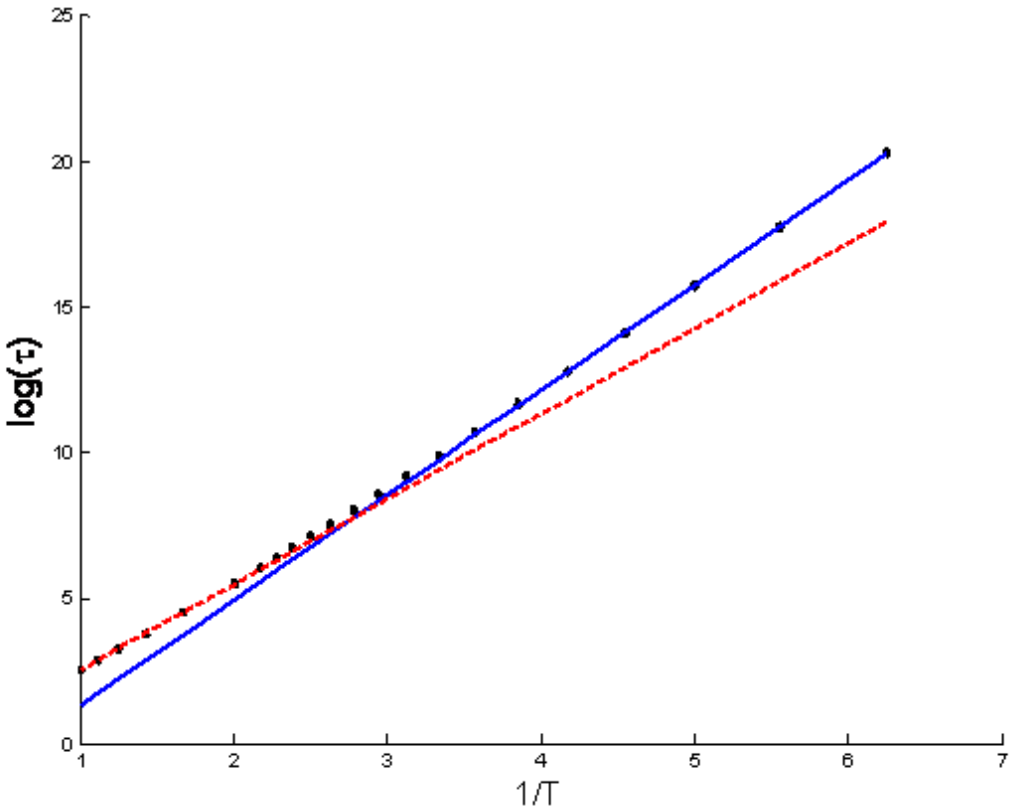

Figure 2.4.4-2: Exponential fits of relaxation time in low and high temperature data
Separate Arrhenius fits to the (—) lower temperature ($0.16 < T < 0.2$) and (--) higher temperature ($0.5 < T < 1.0$) data highlights the changes in relaxation time temperature dependence. Some adjacent data points continue to be well fit, but there is gradual change indicating fragile behavior in the window between the two regions.

To highlight that there is a cooperative relaxation temperature regime flanked both at high and low temperature by simple, non-cooperative relaxation, we fit the high and low temperature data to separate Arrhenius fits. Notice in Figure 2.4.4-2 that the activation energy of the two fits is different, however, both are on the order of the energy required to break three bonds (low T, $E_A = 3.61$, high T, $E_A = 2.92$). At lower temperatures it is elevated, as we would expect. There is no indication of a divergence in the relaxation time of the equilibrium system.

2.5. Supercooled Liquids: Nonequilibrium Glassy States

As expected, the simulation samples prepared using the kMC method and Metropolis MC recipe produce the same results when at high temperatures. However, at lower final temperatures, the simulation samples which are relaxed with kMC develop a change in their dynamics during quenching. We note that if at any specified 'observation time' not all samples will have equilibrated, instead they are arrested at a 'glassy' state. The structure of these low temperature, non-equilibrium samples is significantly different than those prepared with the Metropolis quench. Because we are able to observe the simulation samples, evolution for very long-times, we notice that there is a change in the relaxation behavior at the fragile-to-strong crossover (FSC). Further, we can continue to investigate temperatures beneath the FSC and find that simulation samples will, given enough time, return to equilibrium.

We first establish that our system has traditional glassy behavior by performing a constant rate quench in Sec. 2.5.1. The simulations are terminated when they reach T close to zero. They are not allowed to relax, but presumably would age, if investigated. Our goal is to demonstrate that our model behaves as a glass former and mimics experimental work.

In Section 2.4, we use the Metropolis MC simulations to prepare equilibrium sample for evaluation. We can determine the relaxation dynamics after equilibration using kMC (see 2.4.4). However, the Metropolis MC method does not give us any information about the dynamics during a quench. Thus, we turn our attention to relaxation during quenching at a 'constant temperature' where the simulation is in contact with a heat bath at the final temperature during all steps. Further comparison of the equilibrium samples prepared initially with the Metropolis MC recipe and the simulation samples evolved with kMC, for a

period of time at which some samples seem to have equilibrated and others have not is found in Section 2.5.3. Samples quenched with either MC method appear to have the same characteristics as we would expect from the condition of detail balance. However, samples that have not equilibrated indeed have structural characteristics which reflect this.

2.5.1. Constant Rate Quenches

We can observe dynamic changes and thermodynamic changes upon cooling in equilibrated samples. However, we are able to observe a clear signature of a traditional glass transition by inducing kinetic arrest with a rapid quench, similar to those performed in the laboratory.

Using the n-step kMC algorithm, we are able to cool the system at a constant rate. The simulation samples are initialized at a random state as before and at $T = 5$, which is a very high temperature in our system. They are then cooled at the rate $\gamma = \Delta T / \Delta t$ by performing a MCS using kMC at the current T. The resulting elapsed time is then used to calculate the new T. As the simulation sample cools, each MCS takes longer and results in a larger jump in temperature. At some point, depending on the quench rate, the temperature jump results in the simulation sample leaving an equilibrium quench path. At this point, the sample has arrested and does not find any more satisfied states. The simulation is stopped when the new temperature is negative. Results from various quench rates are shown Figure 2.5.1-1, with the inset providing fits for each data set and the lowest temperature truncated. It is important to note that we repeated simulations with different initial random configurations at each rate. The discrete nature, particularly where there are large temperature drops, leads to clusters of

points. To demonstrate that these are due to individual runs, not from a single sample becoming arrested in that area, the inset provides fits to each simulation run separately.

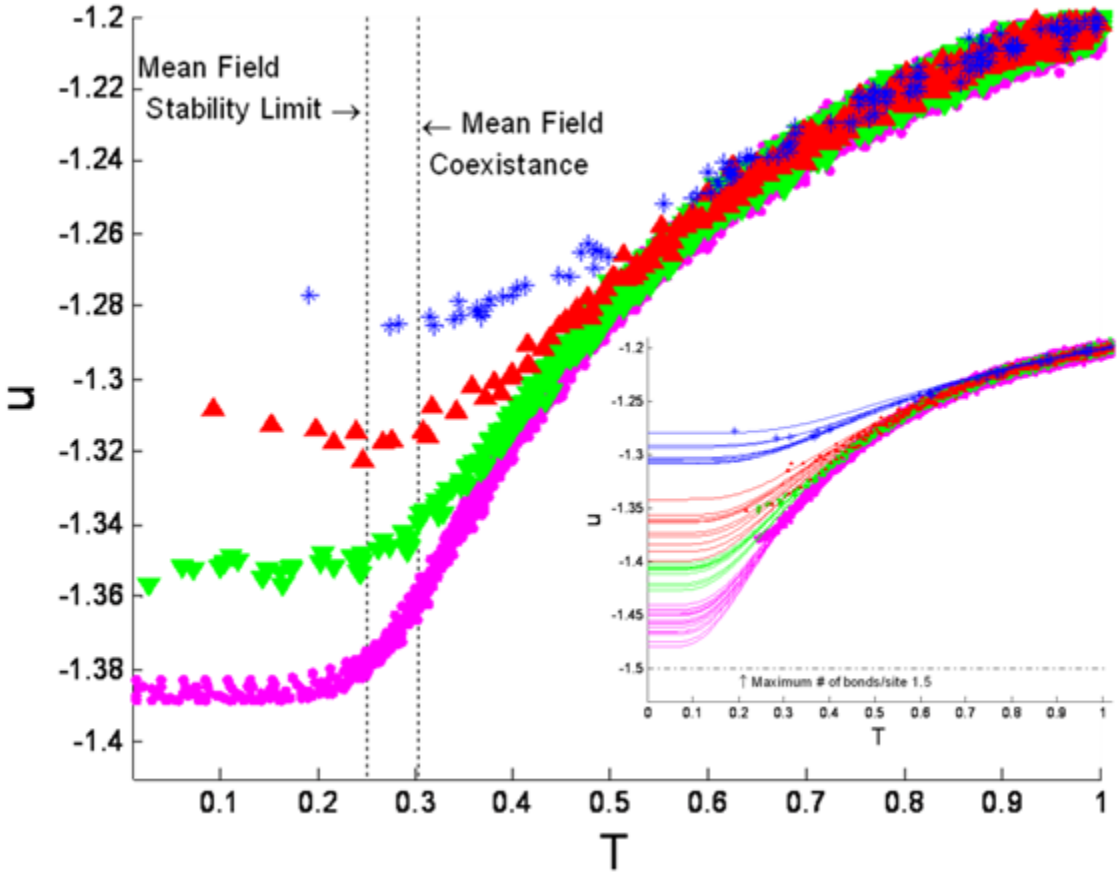

Figure 2.5.1-1: Constant rate kinetic Monte Carlo simulation samples
Energy density as a function of T for 10 independent simulations: γ=0.01(*), 0.001(▲), 0.0001(▼), 0.00001(●). Inset: To emphasize that there are multiple initial conditions simulated each data set is individually fit. We omit the lowest temperature data. The fit is an arbitrary equation similar to Eq. (10) (see Section 2.4.2) without the expectation that the low temperature asympote will be -9/8, intoducing a 4th fit variable: $u = -d - \frac{3}{8}\left((a)\tanh\left(\frac{b}{T}\right) + (1-a)\tanh^2\left(\frac{c}{T}\right)\right)$.

Such behavior is commonly seen in dynamic scanning calorimetry (DSC) measurements in the laboratory. This effect is also captured in several other models[27, 130]. It conforms to the general understanding that a slower cooling rate will prevent the system from falling out of equilibrium at higher temperatures and depress the measured glass transition. Presumably,

an infinitely slow quench would describe the supercooled equilibrium state with the same results as can be found in the previous Section. Therefore, we conclude that we do model a glass forming system and that our results are not the due to some unphysical characteristic of this Hamiltonian.

2.5.2. 'Constant Temperature' Quenches: Evolution with Time

In the context of the energy landscape paradigm, the physical origin of kinetic arrest is generically represented as an inability to relax when trapped in a potential well. Thus, the glassy system has a higher energy than the equilibrium system due to its large number of unbonded molecules. We perform a 'constant temperature' quench by initializing a simulation sample at a random configuration and running the kMC simulation against a constant temperature heat bath. Thus, the energy of the transition states are constant. The exploration of the PEL by the simulation sample leads to a low energy state, which is not discernible from the equilibrium state (as determined by our metrics thus far) if the simulation is run for long enough time.

In Figure 2.5.2-1 the evolution of the energy with time at a given temperature is plotted on a semi-log plot. The range of time scales for the simulation samples to reach their final energy is dramatic. In order to determine whether the low temperature patterns that we see are independent of the choice of initial state or highly dependent on individual quench pattern, additional simulation samples were quenched at $T = 0.16,\ 0.14$ and 0.12 These temperatures were chosen as the samples evolved sufficiently to see their long-time behavior during the 'observation time' of our simulations, but would be most sensitive to their immediate environment on the PEL. There were some deviations in the curves of separate samples quenched under the same conditions as we would expect from diffusion over

different regions on the PEL, but they are small; and, overall, the relaxation paths coincide as can be seen in the figure.

Initially, all the samples relax quickly, as they are very far from equilibrium. Following this preliminary growth in bonding, we observe a very interesting trend. When quenched against moderately low temperature baths, above $T \approx 0.3$, the simulation samples follow a single curve as approach they their long-time energy values. We note that these values are very similar to those which are very close to the equilibrium values found by the Metropolis MC, consistent with the hypothesis that these kMC simulations are also in equilibrium. Neglecting the initial portion of the quench, we also find that the simulation samples approach their final equilibrium value through a sequence of states which are also in equilibrium, although at a higher 'effective' temperature. This result is congruent with recent studies of colloidal systems[131, 132].

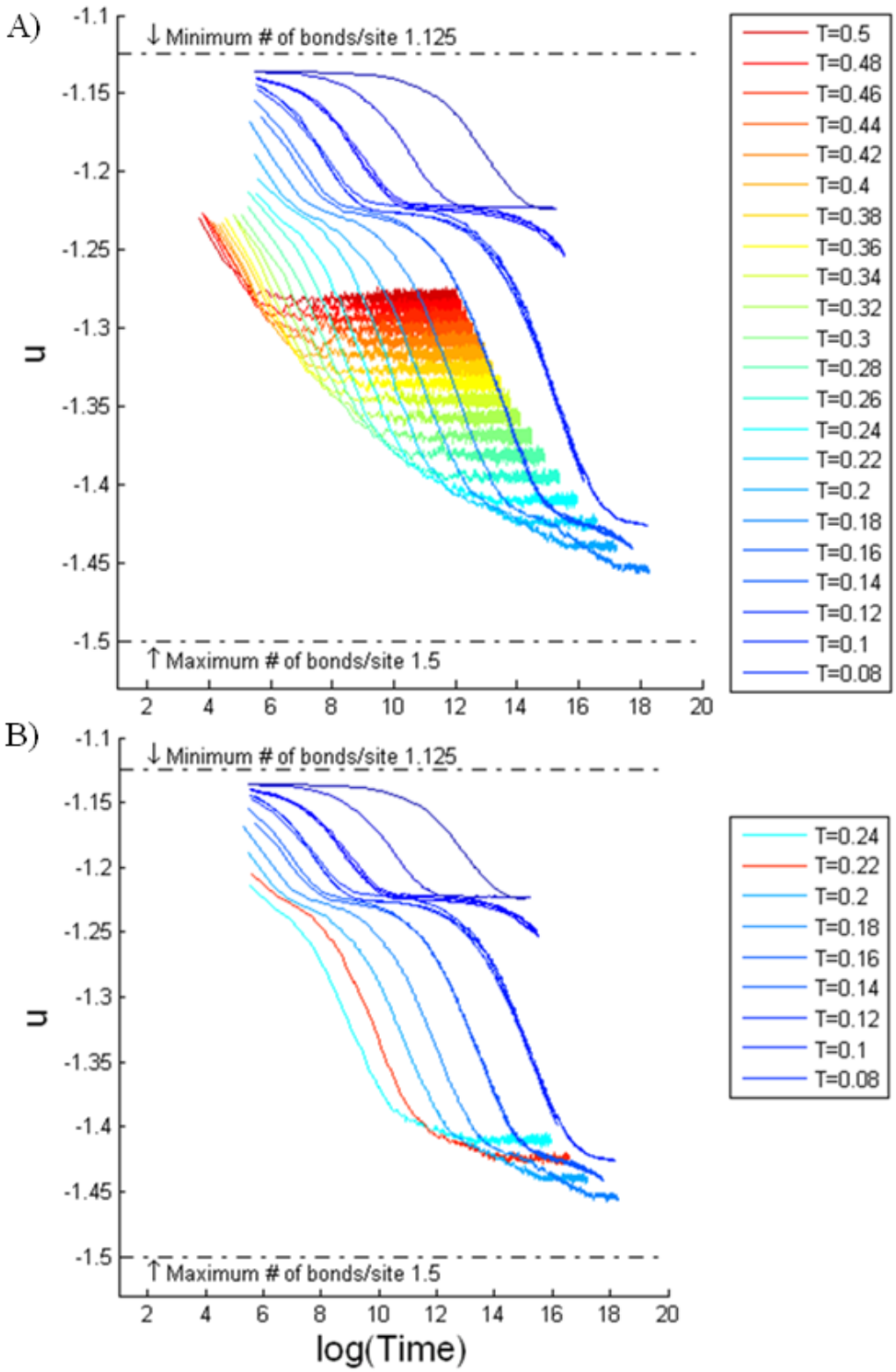

Figure 2.5.2-1: KMC simulation results: 'constant temperature' quench
Starting from a random configuration, kMC was used to evolve samples against a constant heat bath temperature. All quenches, shown in (A) are plotted from high to low by color. A subset of curves are replotted in (B), using new colors for ease of anaylsis by the reader.

In simulation samples quenched against heat baths with lower temperatures, we no longer observe this simple curve. Figure 2.5.2-1 (B) shows a subset of the curves from (A) with a different choice of colors to make inspection of this region easier for the reader. An inflection point can be seen starting at $T_{KMC} \approx 0.24$ such that the simulation sample's energy no longer approaches the equilibrium value in an asymptotic fashion with time. The energy remains relatively constant during two different windows in time, visually appearing as plateaus on the graph. This indicates that there is a kinetic reason these simulation samples become arrested during observations on this time scale, exploring the PEL at that energy for a significant length of time. This multiple step phenomena, in which there are distinctly different dynamics during separate time scales as the simulation sample quenches towards equilibrium, may be reflected in the relaxation dynamics of samples after they have equilibrated. We note that there was indication of such a change in the temperature region same region in Section 2.4.4

Several explanations have been proposed for this phenomena. Caging, in which some molecules are surrounded by immobile molecules that allow changes only on long-time scales has been proposed as an explanation for the development of plateaus in other models[3, 133]. Alternately, this feature may represent regions in which the heat bath temperature is sufficiently low such that the energy required to break one, two, or three bonds becomes significantly different. This would cause the kinetics to change as the sample evolves to lower energy via pathways requiring fewer bonds breaking and more 'diffusion' of vacancies. We speculated in our previous work[1] that this may be the mechanism behind a fragile-to-strong crossover (FSC).

2.5.3. 'Constant Temperature' Quenches: Glassy Structure

It is interesting to compare the domain size for the simulations samples quenched using kMC with those for the equilibrium cases created with the Metropolis MC (Section 2.4.3). All the measurements are made at the end of the respective simulations. When the kMC simulations appear to reach equilibrium, we find that the expectation value of the domain size is similar to that of simulation samples equilibrated with the Metropolis MC method. However when the final state of the simulation is not yet at equilibrium and the sample is considered arrested or glassy, the expectation value of the domain size becomes much smaller. Thus for the kMC simulation samples, the domain size does not grow monotonically with lowering heat bath temperature, but instead deviates when the simulation sample is arrested on the observed time scale. Equilibrium simulation samples should be the same regardless of what choice of transition probabilities is chosen, as long as they meet the condition of detail balance, so this is the result we expect. At $T_{kMC,structure} \approx 0.18 - 0.16$ the domain size begins decreasing with temperature. This is the same region in which the final values of the energy no longer reach the equilibrium value, but instead have fewer bonds.

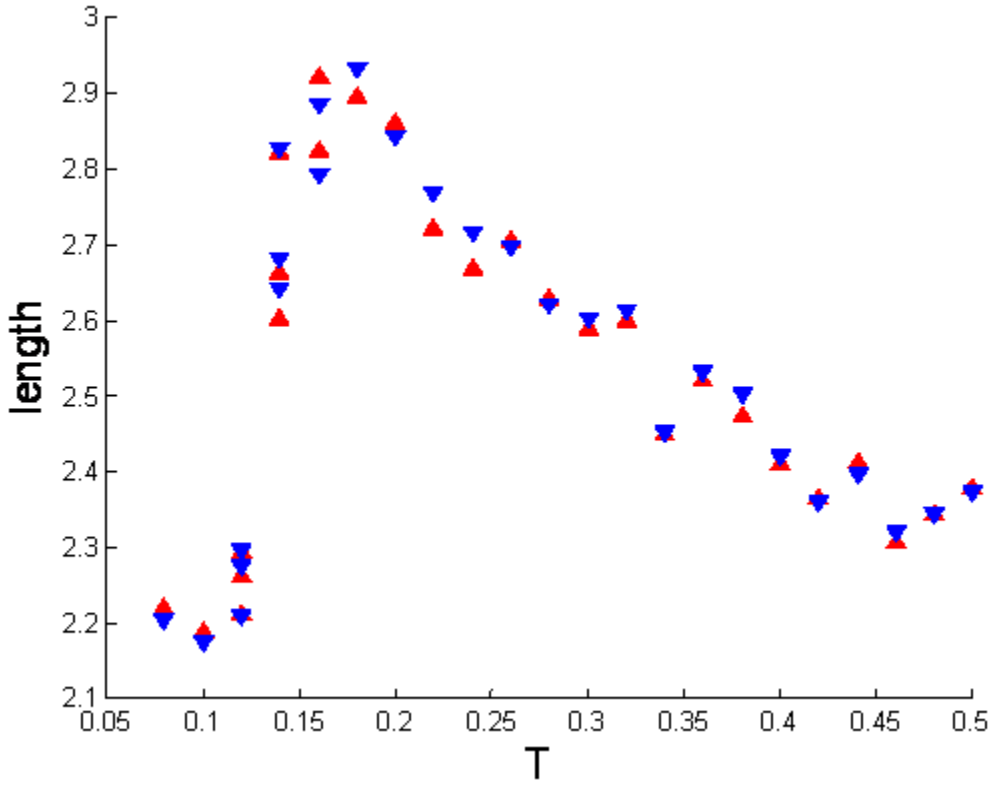

Figure 2.5.3-1: Expectation value of the domain size at different temperatures
The expectation value of the domain size in the direction of the long axis(▲) and perpendicular to the long axis(▼).

We have stated earlier that the formation of these regions is not a thermodynamic property, but instead, the result of the preferred kinetic pathway as the simulation sample traverses the PEL. What is the source of the structural change? We know that the overall energy of the glassy simulation samples is higher than predicted at low temperature as compared with the equilibrium configurations. Thus, it is a requirement that there be a lower density of bonds, which would inhibit large aligned regions. Additionally, it may be that there are pathways on the PEL which are no longer accessible, or are extremely unfavorable due to the separation of time scales between processes which break different numbers of bonds. This comparison demonstrates that there is a distinct difference in the kinetics between the equilibrium and non-equilibrium simulation samples as reflected by the resulting structural features.

2.6. Dynamic Heterogeneity: Evidence of Cooperative Motion

Currently we have two conflicting views of the length scale. First we demonstrated that the equilibrium supercooled liquids have an increasing domain size (Section 2.4.3) starting near the temperature at which we begin to observe cooperativity. This length scale increases in a linear fashion as $T \to 0$, without either diverging, or showing a change at the FSC. We see activated dynamics and a clear stretched exponential bond relaxation function (Section 2.4.4) as the temperature is lowered in the same region the domain size begins increasing. However, we see at the FSC a return to Arrhenious behavior, suggesting length scale has no impact below the FSC. This naturally leads to the question of how these two sets of measurements are related. Particularly, since there seem to be at least some spatially dynamic heterogeneity (SDH) implied by the use of the stretched exponential, characterization of these relationships between length-scale and time-scale are important. In Section 2.4.3, we used the bond relaxation time, τ_{bond} for our analysis of the system dynamics, however, concurrent measurements demonstrated the same trends and similar numeric values in the orientation relaxation time, $\tau_{orientation}$. As the domain size was determined based on orientation, we will monitor the change in the orientation with time during this analysis.

We can quickly see that the dynamics suggest a non-trivial relationship between the length-scale and time-scale. The limitations of our system have not yet made a formal analysis of this system relevant; however, we do find the mathematical description useful in describing our work. The fundamental correlation function now involves a four point correlation function, the change in length scale (two points) and the change in time scale (two points).

We are able to visually establish the presence of spatially correlated dynamics in our model. In Figure 2.6-1, we show a (40 x 40) set of vertices from the larger simulation lattice. We report the time for the molecule at each vertex to change orientation for the first time after an arbitrarily selected time, t_o. To compare each sample despite the disparate time scales at the three temperatures, we choose to represent the time to change orientation at each vertex relative to the distribution of times at that temperature alone. For clarity, we group the molecules into quintiles based on the time for each molecule to change orientation for the first time.

We observe the length scale of spatially correlated motion grows as the temperature decrease. In particular, there are fewer regions which have a checkered appearance, which arises from individual molecules on neighboring vertices changing orientation at time intervals greater than 20% apart. While the choice of the characteristic relaxation time is nontrivial (as discussed below), the increase in the size of dynamic heterogeneities is predicted by kinetically constrained models[28].

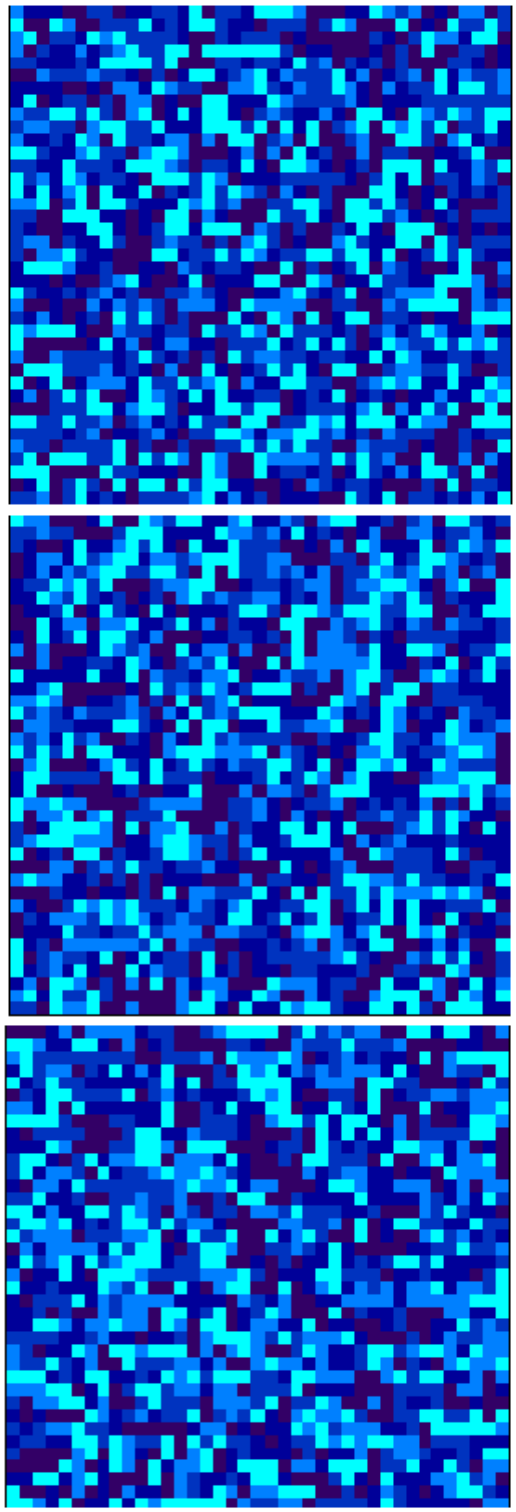

Figure 2.6-1: Representative of supercooled samples, time to first rotation
The time required to for initial rotation of a molecule at each vertex within an equilibrated simulation is roughly distributed in 5 Sections, from shortest to longest, to emphasize the spacial distribution: (■) ~first 20%, (■) ~ 20-40%-,(■) ~40-60%,(■) ~40-60%, (■) ~longest 20%. From left to right $T = 0.4,\ 0.3$ and 0.2 (each sample is normalized separately).

The representation in Figure 2.6-1 highlights the changes in movement along the PEL that occur as the simulation temperature decreases. At moderate temperatures, the simulation sample can still overcome the energy barriers involving breaking several bonds. Thus, the time for a molecule to change orientation for the first time is not as strongly dependent on the recent changes by its near-neighbors as it will become at lower temperatures. This is similar to the observation that the domain size is smaller at high temperature.

The relaxation time data in the range of $T = 0.4$ and and $T = 0.3$ suggest fragile dynamics, and therefore, cooperativity. In this regime, the number of bond influences the motion of a molecule. Thus a change in the orientation of a molecule may facilitate or hinder the orientation changes of its near-neighbors. However, we continue to see a growth in the size of the correlated domains as the temperature cools past the FSC to $T = 0.2$. This region has Arrhenious dynamics and should not necessarily demonstrate SHD.

We have not yet addressed the question whether there are 'fast' and 'slow' regions. Are there spatial groupings of molecules that continue to remain mobile and change orientation quickly with respect to other regions of the lattice? It is possible to evaluate the mobility of an individual vertex by checking whether the molecule is more likely to change orientation again immediately after it changes for the first time. We do this by recording the time intervals between changes in orientation of the molecule at each vertex.

Evaluating the data for the time between successive changes, we may see that an individual molecule will continue to change orientation many times in an interval, then remain stationary, before eventually resuming a sequence of quick changes. This would be a time-scale of the changes in mobility of an individual molecule, $\tau_{mobility}\left(\vec{i}\right)$. Since the motion of a molecule can facilitate change in its near-neighbors, we may see more, less, or similar spatial

heterogeneity in $\tau_{mobility}\left(\vec{i}\right)$ as we do in $\tau_{first\ change}\left(\vec{i}\right)$, the latter represented in Figure 2.6-1. Further, how are either of these values related to the overall relaxation time of the correlation function we previously measured $\tau_{orientation}$?

We have two cases to consider. If the time scale of changes in mobility of the molecules at all vertices is similar, then we can find the average time scale of mobility $\tau_{mobility}\left(\vec{i}\right) \approx \left\langle \tau_{mobility} \right\rangle$. Therefore while there is SHD, the time for a molecule to change orientation for the first time roughly represents the overall correlation time. We find that $\left\langle \tau_{first\ change} \right\rangle = \tau_{orientation}$. Alternately, 'fast' regions stay 'fast' and there are large spatial heterogeneities with respect to mobility. In this case, the relationship between $\left\langle \tau_{first\ change} \right\rangle \neq \tau_{orientation}$ is much more complicated, as the relaxation time of the correlation function scale would be dominated by molecules which require a long-time to change.

Based on the spatial groupings of the time to the first change of a site (Figure 2.6-1) we find compelling evidence of SHD. The question remains how important this feature is to the overall dynamics of the glass. We record the time between changes in orientation for all the molecules from samples equilibrated at the same temperature as those in Figure 2.6-1 to make sure that we capture the time scale for $\tau_{mobility}(\vec{i})$; this data is collected for 10 times the number of MCS required for the change in orientation to occur. Recording the length of time that each molecule spent in the same orientation, the distribution of relaxation times was then fit to a Gaussian curve, shown in Figure 2.6-2. We can compare these reported times to the relaxation time $\tau_{orientation}$.

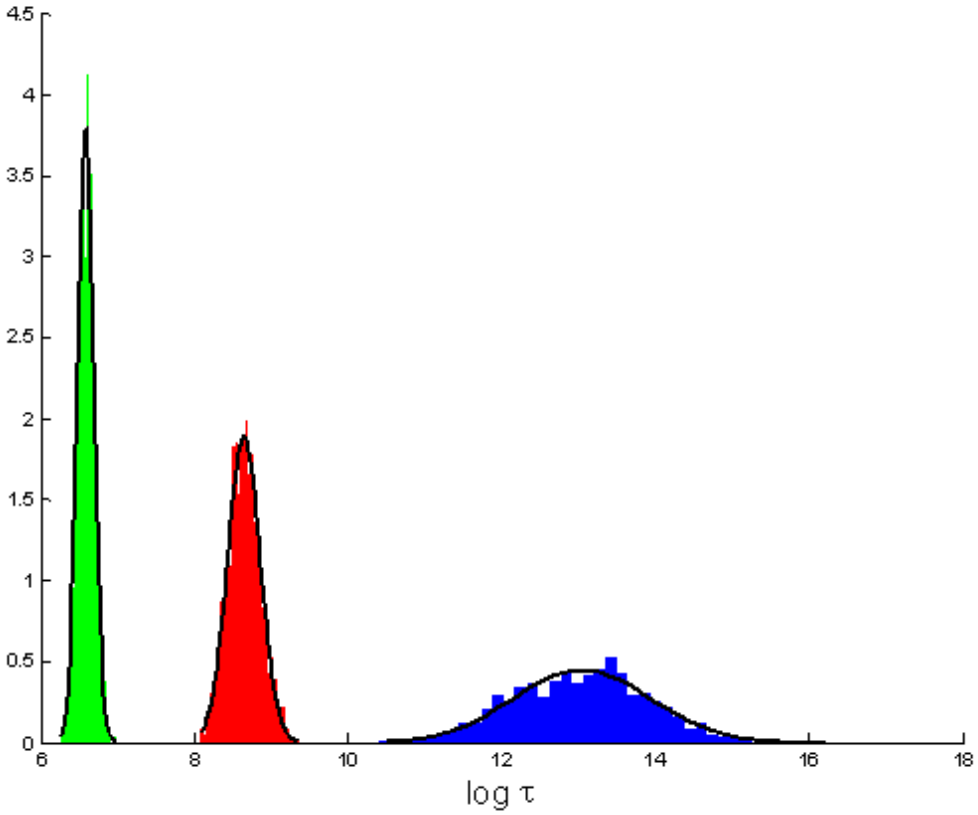

Figure 2.6-2: The distribution of the time for the molecule to change orientation
Tracks the average time it takes for an individual molecule on the lattice to change orientation (units $\log(t/\nu_o)$) for at each vertex, then plots the histogram. The distribution for each sample is well fit by a Gaussian curve with (■) at $T = 0.2$ $(\mu = 13.04\ \sigma = 0.89)$, (■) at $T = 0.3$ $(\mu = 8.64\ \sigma = 0.21)$, (■) at $T = 0.4$ $(\mu = 6.58\ \sigma = 0.11)$.

We can see this from a rough comparison of the overall relaxation times for the entire lattice and the average time to rotation of individual molecules. We report the values of τ_{bond} in Section 2.4.4, which are very close to the values of $\tau_{orientation}$, we discuss here for logical congruency. The integrated relaxation $\tau_{orientation}$ times are 6.97, 9.77 and 15.75, with decreasing temperature ($T = 0.4$, $T = 0.3$, $T = 0.2$). We note that these are longer than the time it takes for the sites to change for the first time indicating $\tau_{first\ change} < \tau_{orientation}$ and that

there is some form of correlation time related to the persistence of the orientation of an individual molecule.

Overall bond percolation, the creation of a geometric network which spans the system, has been shown to occur at temperatures above the glass transition. Indeed, in our system, simulation samples in the fully-dense state will always have a space spanning bond network (Appendix B). Therefore, structural percolation cannot be the signature of the glass transition, nor the sole reason behind the dramatic increase in relaxation times. Alternately, it has been postulated that the increase in modulus at the glass transition is due to percolation of a dynamically slow network of the glass forming molecules, trapping pockets of dynamically fast droplets[87]. This is supported by the idea that the propagation length of mobility is smaller in strong materials than in fragile materials[28] and that the network structure suppress string like motion[134]. While the overall molecule density is constant (every vertex occupied), the bond density is a non-conserved order parameter and may provide the key to unraveling the distributions of fast and slow molecules.

We have attempted a variety of metrics to determine whether there is such a network structure in our systems. In Figure 2.6-3, the average time between changes in orientation for an individual molecule is shown. Those sites that retain the same orientation over a long period of time are shown in red/orange (note time scale on colorbar), so a network of sites which persist for a long-time would appear as a red network. Thus far, we have not identified clear evidence of such behavior. However, this choice would be very sensitive to time scale and our work certainly does not yet exclude the possibility of this dynamic mechanism.

Regions of molecules favoring a specific ordering grow with decreasing temperature (Section 2.4.3). As changes in orientations of highly bonded molecules are strongly

disfavored due to the transition states, it may be that these regions persist for kinetic reasons. This result is consistent with a dynamic viewpoint in which the concentration of mobile molecules is also decreasing[28]. This indicates that the overall relaxation of the system -- the time it takes to no longer carry any correlation with the initial state--would reflect the process required for all molecules to have become mobile. If so the overall exchange rate between slow sites and fast sites, $\tau_{mobility}$, becomes the time scale associated with the overall system relaxation[87, 135]. This time scale may be the same as the relaxation times we calculated, or even longer than that associated with $\tau_{orientation}$ or τ_{bond} and not documented by any of our current metrics. Huang and Richert found that $\tau_{exchange} > \tau_{structural}$ for all temperatures in their experimental system[135]. (This would be equivalent to the statement $\tau_{exchange} > \tau_{orientation}, \tau_{bond}$ in our work.) Further, the length scale and relaxation time scale have been shown to be coupled in a non-trivial manner leading to the necessity for a more complex analysis to fully characterize this form of behavior.

In future work, investigation of SHD could be evaluated for this system, however, we would need to exercise caution to consider the system anisotropy with respect to the i and j axis as demonstrated in Section 2.4.3. The susceptibility of four-point correlation functions has successfully been used to quantitatively demonstrate the relationship between correlation length and relaxation time scale in a variety of systems[134, 136]. However these values would be difficult to extract in our simulations due to the length of time required to capture sufficient information to calculate the appropriate variances. Instead, a recent simplification of the values by using several approximations and the results of the fluctuation-dissipation theorem and the specific heat[128, 137, 138] has lead to the development of metrics using relaxation times and thermodynamic variables which may be more accessible[128, 137, 138].

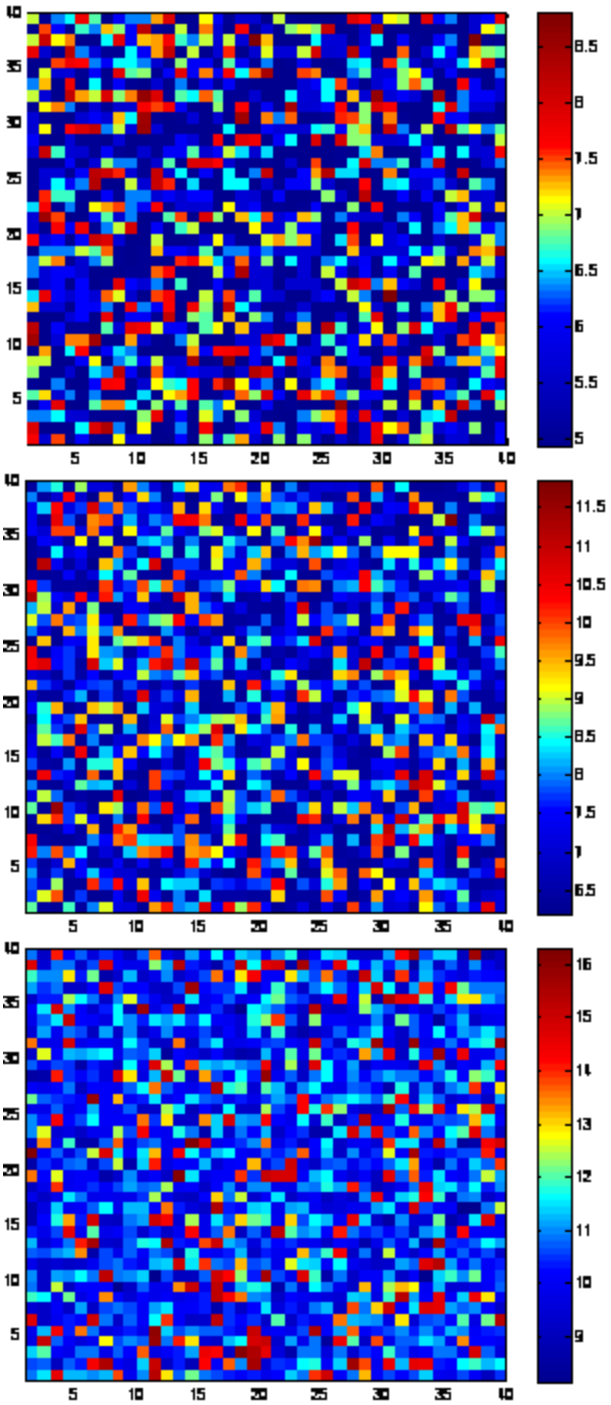

Figure 2.6-3: Representative of supercooled samples, average time to rotation
These figures represent the average time it takes for an individual molecule on the lattice to change orientation (units $\log(t/\nu_o)$) at each vertex, note color bar is a different scale at each temperature. From top to bottom the temperature is 0.4, 0.3, and 0.2 respectively. The fastest times are blue, the slowest red.

2.7. Discussion

Establishing that the simulation samples quenched with the Metropolis MC method were indeed at equilibrium, due to the reproducibility, path independence and correct limiting behavior of the simulation samples, we are able use these samples as a starting point to evaluate low temperature conditions. Additionally, this provides a backdrop against which the deviation of samples quenched with kMC from the known equilibrium behavior may be clearly illuminated. We hope to extract from this comparison an understanding of the vitrification process in our system, establishing relevant temperatures and properties.

A wide variety of temperatures have been identified within this work and a partial list is included here. The subscripts from Chapter 1 have been extended to provide clarity in the context of this discussion.

Temperature	Value	Section Located
$T_{mf,binodal}$	$\left(3\log(3)\right)^{-1} \approx 0.7$	1.4.3[1]
$T_{mf,spinodal}$	0.25	1.4.3[1]
$T_{o,DMF}$	0.24	1.6.2[1]
$T_{\beta,metropolisMC:FSC}$	$\approx 0.24-0.26$	1.6.3[1]
$T_{o,MetropolisMC}$	0.07	1.6.3[1]
T_{Cv}	0.21	2.4.2
$T_{structure}$	≈ 0.5	2.4.3
$T_{\beta:fragility,onset}$	≈ 0.5	2.4.4
$T_{\beta:FSC}$	$\approx 0.24-0.26$	2.4.4
T_o	0.027	2.4.4
T_a	$\approx 0.46-0.5$	2.4.4
T_x	$\approx 0.22-0.24$	2.4.4
T_{kMC}	≈ 0.24	2.5.2
$T_{kMC,structure}$	$\approx 0.18-0.16$	2.5.3

The comparison of all these reported temperatures, both those derived from an analytic approximation and three different simulation techniques, lead to an interesting conclusion. We are able to distinguish three clear temperature regions, with distinctive kinetic properties based on the underlying thermodynamics. We present a synopsis in this paragraph followed with greater detail. In the high temperature regime where the relaxation is Arrhenius, the influence of the transition states and height of the energy barriers has very little impact. As we move to colder temperatures, we find the onset of an activated regime near $T_{onset} \approx 0.5$. Below this temperature, the simulation sample's movement on the PEL becomes influenced by the transition states. We notice that the domain size begins increasing and the stretching exponent reaches its low temperature plateau. The simulation samples experience cooperative relaxation and the orientation of near-neighbors is very important on the motions. The simulation samples also exhibit both kinetic and thermodynamic fragility. We are able to access very low temperatures and see a return to strong behavior, with an increase in the stretching exponent and Arrhenius temperature dependence in the relaxation time. The fragile-to-strong crossover temperature, $T_{FSC} \approx 0.24 - 0.25$, appears to be related to the thermodynamic details of the system. In the next few paragraphs we will weave together the observations that lead us to this description.

At high temperature, the system will move easily over the PEL and explore large regions easily until the thermal energy is on the same order as the bond energy ($T \approx 1$). Below that temperature, the transition states will begin to have an effect and there will be an onset to activated dynamics. In a mean-field description, our model experiences a first-order transition at $T_{mf,binodal} \approx 0.7$, however we don't find this temperature to be a dramatic transition in our kMC results. Instead, we note that by $T \approx 0.5$, which we identify as T_{onset},

a number of results show a clear change in character and signal entry into an activated regime. Thermodynamically, there is no clear change in the internal energy of the equilibrated structures, although the heat capacity increases strongly in this region. Our best indication of thermodynamic fragility is that the temperature dependence of the relaxation time can no longer be well described with a simple Arrhenius relationship, but becomes super-Arrhenius below T_a. We notice this in all three simulation methods. This observation has been found in other models[139], however we note that the critical temperature suggested by the VF fit is very low, e.g. $T_o = 0.027$, foreshadowing that this function does not describe the approach to an ideal glass transition, which would be barely distinguishable from $T = 0$. In this same intermediate range we find the clear kinetic fragility, as well. The stretching exponential β from the fit of the correlation functions, which has been decreasing with temperature, reaches its lowest values at $T_{\beta:fragility,onset} \approx 0.5$. During the temperature range in which the kMC thermodynamics remain fragile, the value of β remains constant, demonstrating that relaxation of the correlation function is clearly non-exponential. We notice that there is a clear onset of a growing length scale of structures on the lattice at this temperature, $T_{structure} \approx 0.5$. This length scale is kinetically, not thermodynamically determined, but does indicate that the near neighbor orientations, as described by the transition states, are beginning to have a large influence.

There is a second important grouping of temperatures reflecting changes in the neighborhood of $T \approx 0.24$, which we believe reflect the FSC. Under the mean-field approximation, the spinodal is the temperature at which the system becomes unstable with respect to the liquid phase and will be trapped in an energy minima in the absence of thermal

fluctuations. During our DMF simulations, we are able to evolve a simulation sample from a homogeneous, supercooled liquid state to a heterogeneous, low energy minima via a very small perturbation. The critical temperature of a VF fit in the DMF simulations $T_{o,DMF} = 0.24$ is very close to the temperature of the mean-field spinodal ($T_{mf,spinodal} = 0.25$). This would indicate complete arrest of the motion on the landscape if the system did not have thermal forcing available to allow it to escape energy minima.

When we consider the results of the kMC, the change in relaxation time with temperature can also be well fit by an Arrhenius function below $T_x \approx 0.22 - 0.24$, indicating a thermodynamically strong glass former. We see that at $T_{\beta:FSC} \approx 0.22 - 0.24$, the stretched exponential now begins to increase with decreasing temperature, becoming kinetically stronger. (This is similarly observed in the previously reported Metropolis MC simulations where $T_{\beta,metropolisMC:FSC} \approx 0.22 - 0.24$ despite the omission of the details of the transition states). We do not observe a dramatic change in the slope of domain size, indicating that there is not a diverging static length scale that at the FSC.

We've established that, for our model, there is an increasing, but not diverging, static length scale for simulation samples equilibrated at decreasing temperature and the entropy remains positive for all temperatures. These observations would seem to indicate that there is not a thermodynamic glass transition for this class of models. Instead, glass transition only occurs when there is insufficient relaxation time to reach an equilibrium state. However, the FSC does have an important thermodynamic signature, the maximum in the heat capacity. Additionally, initial calculations of the minima of the PEL, identified by finding the inherent structure of the simulations (Appendix G), appear to follow the pattern observed in that of

liquid silica at the FSC[72]. If we can cool equilibrium liquids below this temperature, and in the absence of other indicators, how does the FSC relate to T_g ?

A purely kinetic description does not explain a subtlety we see when cooling a simulation sample with the kMC methodology. Above the FSC, as a simulation sample cools at constant temperature, the energy will decrease at the same constant rate, regardless of the temperature until it approaches the equilibrium energy of the final temperature. Then it slows and asymptotes into a smooth master curve, terminating at its equilibrium energy. However, at the FSC, the change in energy with time begins to show plateaus, suggesting that the simulation sample is experiencing significant changes as it traverses the energy landscape. There appears to be an inflection point in the curve of time it takes to reach equilibrium. Under the constraints of our simulation time, some of the low temperature samples reach equilibrium while others do not. However there is no indication of a particular reason they could not reach equilibrium should we continue to run the simulation for even longer times. For those samples which reach equilibrium above or below the FSC, the expectation value of the structure length is similar to the equilibrium structures which were equilibrated with the Metropolis MC. Thus there is no indication that the simulation samples are different at equilibrium applying from applying different transition states during MC simulations, a result consistent with the detail balance requirement.

This leads us to a very interesting image of what might be happening in some structural glass systems at very low temperature. Invoking the energy land perspective, one may consider the variety of paths that a simulation sample may traverse in proceeding from one energy minima to another. If a random thermal forcing can create as little as one pair of molecules which are not fully bonded, then the simulation sample can travel from one

initially fully satisfied state to another skirting many higher energy regions. This process is diffusive in nature, which suggests the source of the Arrhenius temperature dependence as the simulation samples wander in the ravines which connect the energy minima.

Conceptually, our model is always ergodic, however energy barriers may make the system effectively non-ergodic by inhibiting the complete exploration of the PEL at low temperatures, a feature observed in other kinetically constrained models[27]. In those systems there is explicit frustration which causes the glassy dynamics. While certainly exploring portions of the landscape with high potential energy becomes exceedingly rare at low temperature, even at very low temperature the number of degenerate ground states is greater than exponential. Additionally all of the minima are connected via low potential energy pathways on the PEL, unlike those in other systems. Therefore, we do not see the configurational entropy disappear at finite temperature.

The development of a plateau in the relaxation dynamics from a random configuration to a low temperature minima at the fragile-to-strong crossover is a feature that calls for additional exploration. One possibility is certainly that the population of unbounded molecules peaks in these simulations. It is shown in Appendix E that the distribution of these molecules is a non-monotonic function of temperature. Their presence makes the progress of the simulation exceedingly slow computationally, but this does not have the same dramatic effect on the 'real time' which we document. However, this may hint at underlying structural features that lead to the system becoming trapped at higher energy states for a long length of time. This indicates that documenting the population of molecules which have 0, 1, 2, or 3 bonds may give insight into these issues. When considering only the potential energy landscape, we should recall that it is not the internal energy alone, but the free energy with its

entropic component, that describes the equilibrium state[140]. Therefore, we need to consider large, flat regions on the landscape that may describe barriers due to entropy alone, in which case it may never be necessary to take an energetic step up-hill[141].

An alternate idea that involves percolation considers accessibility of regions on the PEL directly[142]. In this theory, transitioning into the glassy state occurs when the possible paths which a simulation sample may follow between minima on the landscape no longer percolate. Because the PEL is hyper-dimensional, the mean-field approximation of this transition becomes exact and predicts the correct behavior at the critical point[142]. We have not formulated our mean-field approximation to address a PEL percolation transition; to do so we would need to include the details of the transition states and consider a time variable. However our static representation may still capture some of this flavor because it does consider the temperature at which amorphous energy minima are preferred with respect to the liquid (random) state, $T_{mf,binodal}$, as well as when the simulation sample will be confined to energetic minima, $T_{mf,spinodal}$. This approach is similar to that described in the Introduction, which describes the simulation sample trajectories that lose ergodicity on time scale of the simulation[108] and those that involve tree representation of movements[110].

Other models with limited valency or 'patchy' interactions have recently been studied. Among the findings, we see that a number of gelformers have transitions influenced by their structural orientation including proteins[143] and colloids[92]. Beyond the scope of this set of materials, valency is also found to be a crucial detail in some materials with a liquid-liquid phase transition, which is not a spatially homogeneous gas/liquid separation, but instead a heterogeneous phase change between two different locally oriented structures [4, 107].

Additionally, the number of bonding sites or patches appears to have more influence on this behavior than the location of the interaction although both contribute to the phase diagram[143]. The overall effect of increasing the valency is to increase both the critical temperature and density when considering phase separation[143]. Our phase diagram is similar to those found both experimentally and in other simulation models. Indeed, without valency limited potentials in colloidal systems there is not a low temperature region that would be able to generate a disordered homogeneous (as opposed to phase separated) arrested state[7, 17]. The lower the valency in these systems, the smaller the force for phase separation as most of the particles are fully bonded so there is no drive towards further density increase. The possibility of finding a region in which the low temperature promotes long-lived bonding opens up exploration of colloidal gels[133, 144].

Currently, in our model we do not have a preference for a crystalline form, however we could easily modify the Hamiltonian by inducing a field

$$\beta H = -\sum_{\langle \vec{i},\vec{i}' \rangle} \beta\varepsilon\left(\sigma_\alpha\left(\vec{i}\right)\sigma_\gamma\left(\vec{i}\,'\right)\right) + \sum_{\vec{i}} \beta\mu_\alpha\sigma_\alpha\left(\vec{i}\right)$$
$$\text{where } \mu_\alpha = \begin{cases} 1 \text{ if } \alpha = 1 \text{ or } 3 \\ 0 \text{ otherwise} \end{cases} \tag{18}$$

or non-equal bond energies:

$$\beta H = -\sum_{\langle i,i' \rangle} \beta\varepsilon_{mn}\left(\sigma_\alpha\left(\vec{i}\right)\sigma_\gamma\left(\vec{i}\,'\right)\right)$$
$$\text{where } \varepsilon_{mn} = \begin{cases} \varepsilon_{ll} \text{ if two long axis bonding sites fall on same edge} \langle i,i' \rangle \\ \varepsilon_{ls} \text{ if a short axis and a long axis bonding sites are along edge} \\ \varepsilon_{ss} \text{ if two short axis bonding sites fall on same edge} \langle i,i' \rangle \\ 0 \quad \text{otherwise} \end{cases} \tag{19}$$

Vogel and Glotzer[134] found that the length scale of clusters did not diverge at the FSC and that there was no clear indication that this temperature was linked to spatially heterogeneous dynamics. However, they point out that the valency would have a strong effect on the spatio-temporal mobility of particle motion because the imposed network structure statistically limits the number of number of near-neighbors which are mobile. Our T-shaped molecule model can easily be extended into higher dimensions (Appendix D) or studied on other lattice structures. Additionally, changing the bonding site number and locations on the molecule does not require any modification of the fundamental techniques.

Our model could be considered one of a class of models which limits the number of near-neighbor bonds via defining the properties of the molecule at the vertex as having fewer bonding regions than the number of edges of the lattice. This leads to viewing the overall state of the system as a composite of the individual occupancy and orientations at each vertex. A conceptually similar Hamiltonian is under very active investigation. A limited valency system is created by restricting the number of bonds via exclusions of states of the system which have too many bonds converging at a single vertex (or too many near-neighbors)[113]. Models similar to ours, in which the valence restriction is a property of the molecule, may prove computationally faster during simulations because we can create 'look-up tables' enumerating, *a priori*, every combination of near-neighbors. Thus the calculation of energy of a state progresses via matrix multiplication. Formulations restricting the number of bonds at a vertex require a step identifying whether the new state is possible, which requires comparisons, inherently slow computationally. One way to side-step these issues is to map the restriction onto a model in which all occupation states are possible, but create an energy penalty for vertexes with large number of near-neighbors. In the limit of an

extremely high penalty, we should recover the original exclusion of states. This also suggests a mechanism for proving that the two classes of models may be mapped to each other.

With the simplicity of this model, the possibility of analytic explorations is enticing. It is interesting to note that Sastry et al. found that the Bragg-Williams approximation was better at describing the skewing of the liquid gas spinodal to the low density side of the phase diagram than the Bethe-Peierls approximation in this class of models[113]. However, no explanation for this was proposed. In our model, this skewing was the result of the phase separation between the gas and a heterogeneous liquid phase. It might be that the implementation of the Bethe-Peierls suppresses or excludes consideration of this phase. However, because within their work no explicit discussion of the implementation which would distinguish between an homogeneous and heterogeneous liquid is included, this explanation is tenuous at best. An implementation of the Wertheim perturbation analysis was restricted to valencies above 3 and below 5, severely limiting this approach for exploration of a larger number of systems[144]. With the simulation work in hand, extension of the analytic description of the model can be better approached.

2.8. Conclusions

Our strikingly simple model can be used to describe the low temperature behavior of valence-limited glass formers. Employing the Metropolis MC method, we can cool simulation samples to equilibrium providing the starting states for study of the thermodynamics, dynamics and structure. Consideration of results from the evolution of the simulation samples with a kinetic MC recipe, thus including the effects of transition states on the sample motion on the PEL, yields a picture of three distinct dynamic regimes. At high

temperatures the system is free to move without significant impact of the transition states. However, as the system cools, it reaches T_{onset} below which activated events become important, the sample motion that must overcome an energy barrier by concerted thermal activation. In this region we find that the relaxation time exceeds that of a simple Arrhenius dependence and the structural length scale increases. In our model both are hallmarks of a fragile glass former.

Further cooling results in a fragile-to-strong crossover in our system at T_{FSC}. Below this temperature, the stretching exponential increases in value and the relaxation time returns to an Arrhenius behavior with cooling. The FSC resolves the Kauzmann Paradox by demonstrating that the extrapolation of the fragile properties above T_{FSC} is not valid as $T \to 0$. Instead, we find that the configurational entropy does not disappear at low T.

As is found in experimental systems, we can force our system into non-equilibrium conditions by quenching a random sample with the kMC method at a constant rate. However, when a random simulation sample is allowed to cool against a constant temperature bath we observe that it will eventually reach equilibrium. We follow the potential energy as the system cools as a function of time. We see a change in the cooling behavior around the FSC. At higher temperatures, the sample cools rapidly until it asymptotes to the equilibrium temperature. The overlay of this behavior at different temperatures leads to a cooling curve, along which all the samples are at equilibrium at the appropriate potential energy as the time progresses. Near the FSC we note that there is the onset of a plateau at higher potential energies, indicating the simulation sample experiences a multi-step relaxation process where it is no longer at equilibrium as it is cooled. There is no evidence, however, that the samples will not eventually reach equilibrium. It does suggest

that on the time scale of experimental and simulated observations, the lattice is arrested at in a non-equilibrium state with higher potential energy. We identify simulation samples that are at this temperature plateau as glasses, indicating that T_{FSC} may often be identified as T_g.

During the simulations which are evolved from an initial, equilibrated state with the kMC method, we observe a peak in the heat capacity at the FSC. Additionally, as we observe the structure of the system, it begins to become aligned due to kinetic reasons starting at T_{onset}, but does not show evidence of a static length scale divergence with temperature. At low temperatures, simulation samples that would be characterized as arrested, glassy states show a significant decrease in static structuring. Our model appears to show significant spatially dynamic heterogeneities, with an increasing correlation length as the temperature decreases. There is evidence that the evolution of the system is dominated by mobile molecules that can change their orientation quickly, and that the time for structural relaxation is determined by the time scale of exchange of mobile and immobile molecules.

The kinetics and thermodynamics of self-assembled structures is a rich field for research today. Our model allows us to explore low temperature conditions at long-times, resulting in insight into the class of limited valency systems. In previous work we have extended this model into a two-phase regime and identified a large variety features in the gel phases upon the addition of solvent. Similar work could lead to a deeper understanding of the phase behavior of physically reversible gels and illuminate the relationship between the glass transition and gelation.